
POLITECNICO DI TORINO

Master of science program in MECHANICAL ENGINEERING

Master's Degree Thesis

Aerothermal analysis of a Wave Rotor



Supervisors:

Prof. Ferlauto Michele

Dr. Savadori Simone

Author:

BAISEN ZHENG

April 2021

Acknowledgment

I want to say thank you to my thesis supervisors, FERLAUTO MICHELE and SALVADORI SIMONE, for their careful guidance of my graduation thesis in the past few months. Wave rotor is not a popular topic in the field, it is not easy to find rich reference articles for studying and Prof. Michele help me a lot in all aspects related to the topic. Also Dr. Simone spent much time to explain related CFD knowledge for me. They gave me guidance more than the thesis required, which greatly improved my understanding of academic writing and taught me a lot of specific research skills; knowledge is a vast ocean, I am only one of the flat boats.

I am grateful to the teachers who have given me selfless help in those years of development. Let me have a glimpse of the vastness of this ocean. Thanks to the classmates who have given me care and support in life, because of you, university life is colorful. Thanks to my alma mater, who has given me the top educational resources in China, which gives me the opportunity to go abroad, enjoy a more advanced lifestyle, given me a rational look at the world, given me a delicate sense.

Finally, special thanks to my parents and everyone who believed in me and inspired to do even better.

Content

Acknowledgment	b
Content	3
Abstract	1
1. Background and Introduction	2
1.1. Wave rotor configuration	3
1.2. Working principles	7
1.3. Studying history	11
1.4. Recent research and motivation	14
2. Theoretical analysis	21
2.1. Topping cycle	21
2.2. Shock wave	29
2.3. Conservation law	30
2.4. Boundary layer theory	35
3. Model developing	39
3.1. Introduction of software	39
3.2. 3D model building and meshing	41
3.3. Meshing	43
3.4. Model development in Fluent	48
4. Simulation result and analysis	58
4.1. Inviscid model	58
4.2. Viscous model	67
5. Conclusion and further work	79
Reference	81

Abstract

With the development of energy and propulsion industry, there are increasing requirements in the improvement of system performance. Wave rotor, or called pressure exchanger, is a device which has potential to achieve the compression process or as a turbine machine by its unsteady flow process in channels. The technology has shown great power to enhance the performance and operating characteristics of a variety of engines and machinery utilizing thermodynamic topping cycles. Although there have been a variety of applications since the early year, wave rotor is still not widely used and is barely known to engineers due to the imperfect study result so far, which the imperfection is result from the poor measure and analysis tools in the past.

Nowadays, with advanced technology, the research on wave rotor is risen again. The aim of this article is to do the aerothermal analysis to wave rotor. By creating a simple system model with certain geometry and features, then using numerical analysis tool like Fluent simulate the unsteady flow process. Then finally, according to the results, discuss the fluid flow behaviors and thermal behaviors and their influences to the properties of system.

Key words: wave rotor, unsteady flow, numerical analysis.

1. Background and Introduction

The objective of this chapter is to provide a succinct review of past and current research in developing wave rotor technology. This technology has shown unique capabilities to enhance the performance and operating characteristics of a variety of engines and machinery utilizing thermodynamic cycles. Although there have been a variety of applications in the past, this technology is not yet widely used and is barely known to engineers. Here, an attempt is made to summarize both the previously reported work in the literature and ongoing efforts around the world. The chapter covers a wide range of wave rotor applications including the early attempts to use wave rotors, its successful commercialization as superchargers for car engines, research on gas turbine topping, and other developments.

Oscillatory and pulsatile fluid motion is ubiquitous in nature yet, it is relatively poorly studied by engineers despite the invention of cyclically operating engines and machines. The potential for utilizing unsteady flows has been recognized since the early twentieth century, which has been neglected as long as substantive improvements could be made to conceptually simple semi-static devices, steady-flow devices, or crypto-steady devices (having flow that is steady in a particular frame of reference, e.g., turbomachines). Further, the inherent nonlinearity of large-amplitude wave phenomena in compressible fluids necessitates detailed flow calculations, which until recently were too laborious, expensive, or imprecise. By understanding and exploiting complex unsteady flows, significantly better engines and thermodynamic cycles can be enabled for various applications.

Since the first industry revolution occur, every time the development of thermodynamic cycle has led to a huge increase in industrial productivity. Similarly, nowadays, thermal machine has still played an important role in people's daily life. There is a continue demand of increasing the performance of thermodynamic cycles for the development of industry.

The traditional methods, like using compressor, are based on steady-flow process to improve the fluid condition so that the whole thermal machine system could obtain better performance. Comparing to steady-flow process, unsteady-flow process has been proved that for the same inlet and outlet Mach numbers it has better performance in pressure gain ^[1]. Thus, in past thirty years, it has been concerned by researchers continuously.

Shock tubes, shock tunnels, pulse combustors, pulse detonation engines, and wave rotors are a few examples of unsteady-flow devices. The basic concept underlying these devices is the transfer of energy by pressure waves. By generating compression and expansion waves in appropriate geometries, wave machines can transfer energy directly between different fluids without using mechanical components such as pistons or vaned impellers. The major benefits of these unsteady-flow machines is their potential to generate large pressure changes in short time or distance^[2,3], and to tolerate transient peak fluid pressures and temperatures that exceed continuous exposure limits.

1.1. Wave rotor configuration

The essential feature of a wave rotor is an array of channels arranged around the axis of a cylindrical drum. As schematically shown in Fig 1.1.1

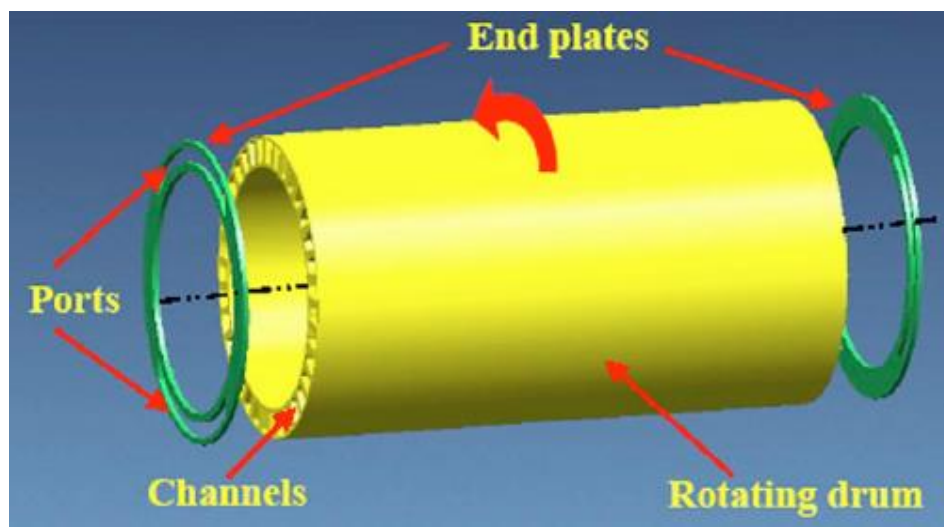


Fig 1.1.1 Schematic configuration of a typical wave rotor

the drum rotates between two stationary end plates, each of which has a few ports or manifolds, controlling the fluid flow through the channels. Through rotation, the channel ends are periodically exposed to differing port pressures, initiating compression, and expansion waves within the wave rotor channels. The number of ports and their positions vary for different applications. By carefully selecting their locations and widths to generate and utilize wave processes, a significant and efficient transfer of energy can be obtained between flows in the connected ducts. Thus, pressure is exchanged dynamically between fluids by utilizing unsteady pressure waves. Unlike a steady-flow turbomachine that either compresses or expands the fluid, the wave rotor accomplishes both compression and expansion within a single component. To minimize leakage, the gap between the end plates and the rotor have to be very small, but without contact under all operating and thermal expansion conditions. An inverted design with stationary channels and rotating ports is also possible^[4]. Such a configuration may be preferred for laboratory investigations for easy flow measurement in the channels where the important dynamic interactions take place. In practical design, this arrangement is mechanically inconvenient^[5].

Most designs use straight axial channels, but curved channels can be used to create a “wave turbine” that produces shaft power. With axial channels and matched port flow alignment, the power required to keep the rotor at a correctly designed speed is negligible^[5,6], as it only needs to overcome rotor windage and friction. In such a configuration, the rotor may be gear or belt driven or preferably direct driven by an electrical motor ‘not shown’. Alternatively, a self-driving configuration, known as the “free-running rotor,” can drive itself by using port flow incidence on channel walls to turn the rotor^[7,8].

There are several important advantages of wave rotor machines relative to competing turbomachines particularly for straight channel rotors with no shaft power transfer. Wave rotor flows can respond on the time scale of pressure waves with no rotational inertia lag. Their rotational speed is low compared with turbomachines,

unless designed for shaft power generation, which should result in low material stresses. However, the tip shroud offsets this advantage somewhat, and the design must safeguard against fatigue-induced failures in surfaces subjected to cyclic pressure fluctuations. Wave rotor geometry can be mechanically simpler than those of turbomachines, allowing inexpensive manufacture. In addition the rotor channels are less prone to erosion damage than the blades of turbomachines. This is mainly due to the lower velocity of the working fluid in the channels, which is about one-third of what is typical within turbomachines and the absence of flow turning. Another important advantage of wave rotors is their self-cooling capability. In heat engine applications, the rotor channels pass both cool air "being compressed" and hot gas "being expanded" in the cycle at least once per rotor revolution, alternating faster than thermal diffusion rates, allowing peak cycle temperature above materials limits. The rotor temperature equilibrates between the temperature of the cooler air and the hotter gas but may retain axial and radial temperature variation that limits strength and distorts sealing surfaces.

Despite generally attractive features, several challenges have impeded the extensive commercial appearance of wave rotors. Numerous research efforts have been carried out during the past century to understand the complex unsteady flow and creatively select the best wave rotor configuration for a particular application. The obstacles have been mainly of a mechanical nature, such as sealing and thermal expansion issues, as mentioned frequently in this review. Nevertheless, continued impetus for energy efficiency, diminishing advances of older technology, and marketplace changes have stimulated new interest in wave rotor technology.

four-port wave rotor example

The construction of a four-port wave rotor is shown in the Fig 1.1.2, The typical configurations include: the fixed end plates with ports connect to the inlets and outlets; a rotor with channels distributed along the circle and a shell use to locate and protect the rotor.

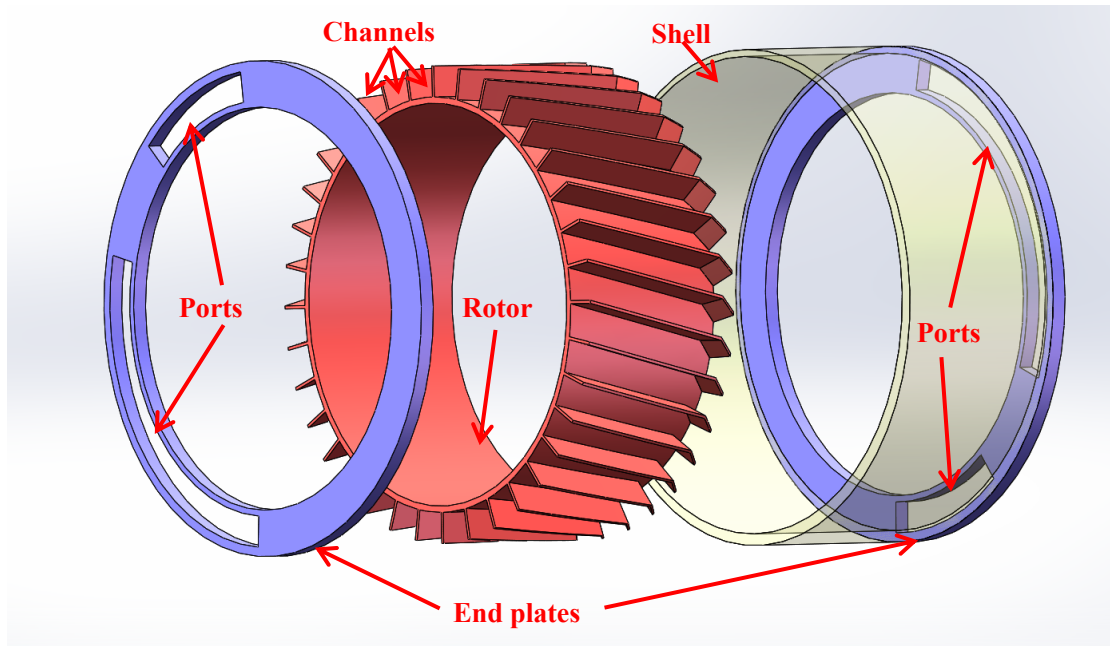


Fig 1.1.2 Schematic configuration of a typical wave rotor

The positions of the ports are design according to the work condition of wave rotor to achieve the best performance. The rotor is usually drove by a shaft, the blades and the walls shape the channels where the pressure exchange occurs. The channel could be straight, helical, or even arc. At the end of channel, there could be a fold which shrink the area of section which forms a nozzle for higher Mach number.

In fact, wave rotor could be classified according to the number of ports. Different number of ports have been developed for different applications. As it was concluded by Akbari^[1], *four-port configurations have been used mainly as superchargers for internal combustion engines. Three-port wave rotors have been employed in pressure dividers and pressure equalizers in which the pressures of different fluids are increased or reduced. Two-port, four-port, five-port, and nine-port wave rotors have been investigated for gas turbine engine topping applications, including some with on-board combustion.* The four-ports wave rotor mentioned above is mainly developed and discussed model and, for more details, Fig 1.1.3 and Fig 1.1.4 show through-flow (TF) and reverse-flow (RF) connections for four-ports wave rotor in the gas turbine system.

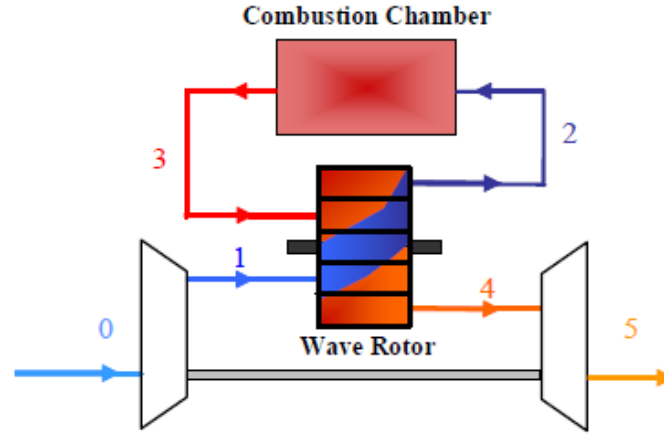


Fig 1.1.3 Through-flow (TF) connection for four-ports wave rotor

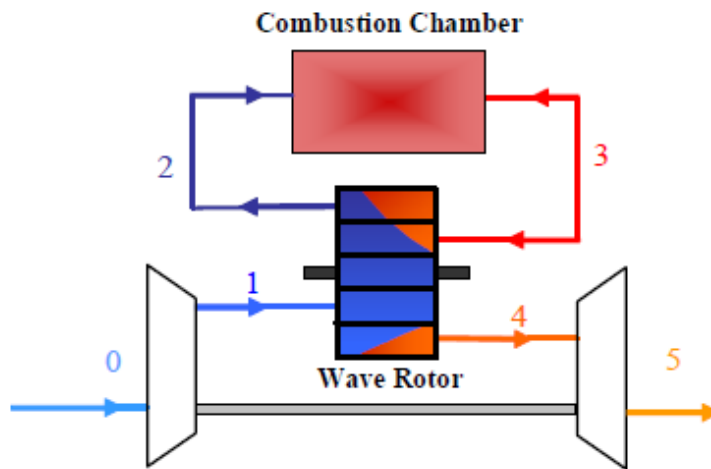


Fig 1.1.4 Reverse-flow (RF) connection for four-ports wave rotor

1.2. Working principles

Different from compressor, wave rotors do not use pistons or vaned impellers to compress the fluid. Instead, wave rotor utilizes unsteady flow, employing compression waves and expansion waves to change energy in appropriate geometries. Take TF connection (Fig 1.1.3) as an example, the fresh air from compressor flow into the wave rotor channels at low pressure inlet port (port 1) first. Then, with the rotor rotation, the high pressure burnt gas from combustion chamber flow in and pressurize the fresh air when channel connect to high pressure inlet port (port 3). When the channels connect to high pressure outlet port (port 2), the pressurized fresh air will leave the rotor and

prepared for combustion. Finally, the residue low pressure burnt gas will flow out through low pressure outlet port (port 4) with free emission process and scavenging process done by fresh air. Since the principle mentioned above is a general description, the details are more complex.

Pressure exchange is the main function of the wave rotor. Weber, H.P. has concluded the principle of pressure rise in his article ^[10], as shown below in Fig 1.2.1, which is a x-t diagram. The vertical direction represents the time variable condition, shows the rotor passes the port as time. The horizontal direction represents the distance variable along axial direction of rotor.

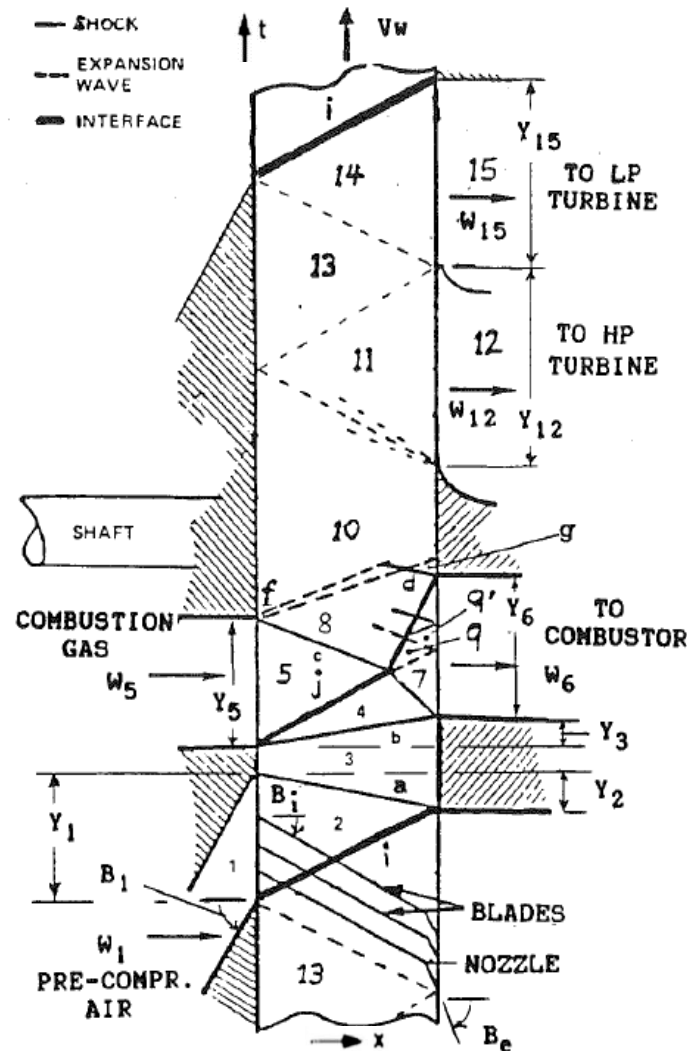


Fig 1.2.1 x-t diagram of a TF connection wave rotor

According to the research, the pressure rise in a four-ports wave rotor is mainly accomplished with four shocks:

-
1. *Shock "a" is generated by stopping the scavenge air flow at state 2 by the blade passages rotating past the stator end wall.*
 2. *Shock "b" is generated by opening the blade passages to the hot gas flow at state 5.*
 3. *Shock "c" is reflected by opening the blade passages to back pressure at state 6.*
 4. *Shock "d" is generated by stopping the air flow from the rotor into port 6 by the blade passages rotating past the end wall. This shock is intersected and weakened by expansion waves that result when the flow is stopped by the blades rotating past the downstream edge of port 5.*

Besides, considering the flow condition, the performance of wave rotor depends on many factors. According to the experimental study in NASA ^[11], at least 3 dominant factors will make influence: “Gradual Passage Opening Effect”, “Viscosity of Fluid” and “Leakage”.

Gradual Passage Opening Effect represents that when the channels are gradually opened and closed to the port during rotation, there would be an influence on the process of wave generation, growth, and propagation. Based on the effect, Koji OKAMOTO ^[12] and his team have developed a 2-D numerical analyses combine with experimental pictures, which the research shows the exist of primary and secondary chock as Fig 1.2.3 shown. Meanwhile, the Gradual Passage Opening Effect is found in the beginning of flow. Then, the article considers the effect of leakage, and represents the difference of two cases, for later condition, the leakage leads more vortex during opening process and as shown in Fig 1.2.4. It is called Multi-passage effects.

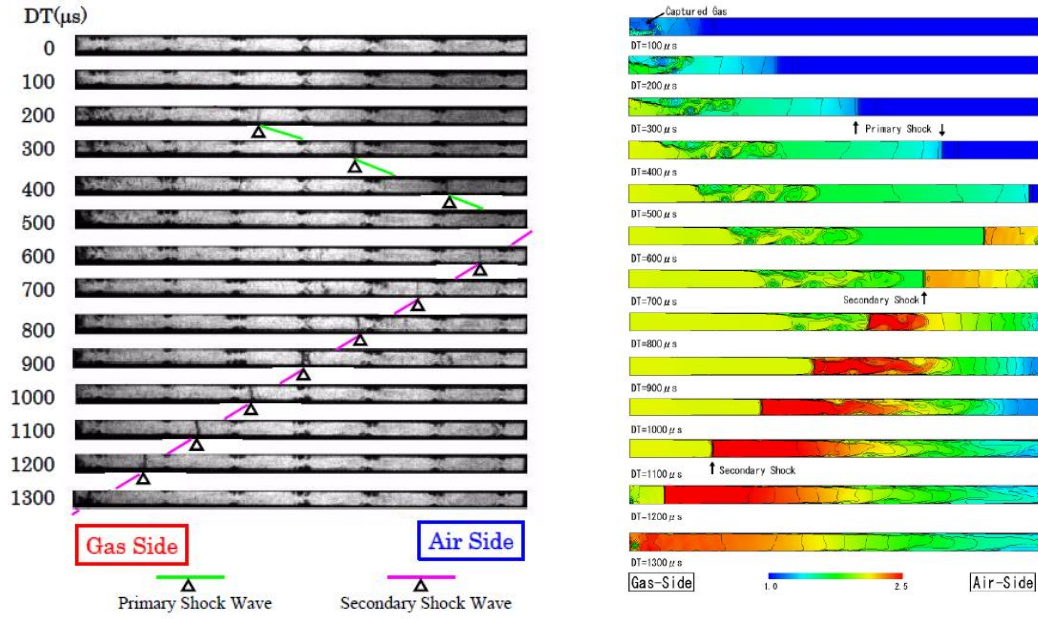


Fig 1.2.3 Schlieren Pictures (Left) and Density Contour diagram (Right)

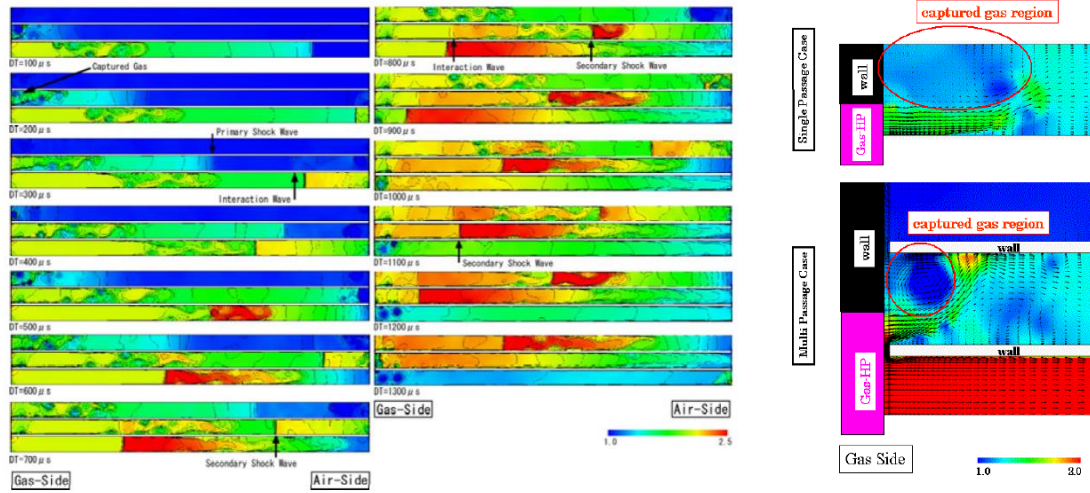


Fig 1.2.4 Density Contour diagram with leakage (Left) and Inflow Difference (Right)

Concentrating on the leakage effect, Akbari ^[13] and his team had a further study on it. They developed a new model considering the leakage paths of the entire device, combining quasi-one-dimensional (QOD) computational fluid dynamics prediction code with a network flow solver.

As shown in Fig 1.2.5, leakage mainly exist between channel and end-wall due to requirement of smooth rotation. However, the different segments connect to different port, where the interface will also have leakage.

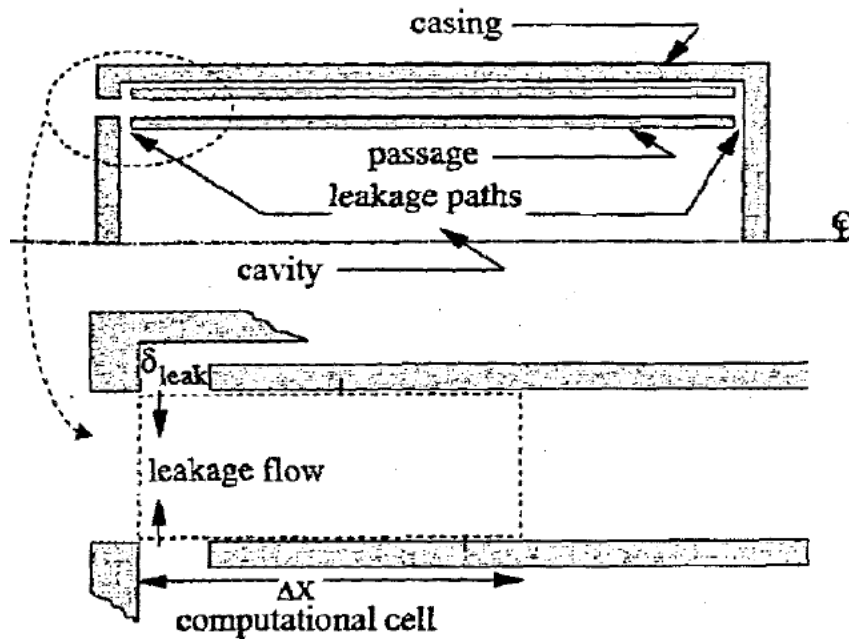


Fig 1.2.5 Leakage flow between channels and end-walls

The model and experimental data both proved that the leakage has a significant effect to rotor performance due to flow losses and heat transfer. But the sealing techniques and other leakage-defeating methods are still in discussion.

1.3. Studying history

In 1900s, the earliest pressure exchanger was proposed. Different from the modern pressure exchanger principles, using pressure wave to pressurize the fluid, the original one consisted of a cellular drum, and it rotates between two end plates, which containing several ports as different pressures inlets and outlets, exchanging their pressure. While, in that stage, it's hard to study the unsteady flow due to poor technique. Until 1940s, Brown Boveri Company developed practical wave supercharger with topping cycle, the wave rotor first showed its great power.

Thanks to the success in the plant turbine, the wave rotor began to be used by many companies and continuously improved. Besides, the wave rotor was also improved and gradually using in the smaller machinery like diesel engine.

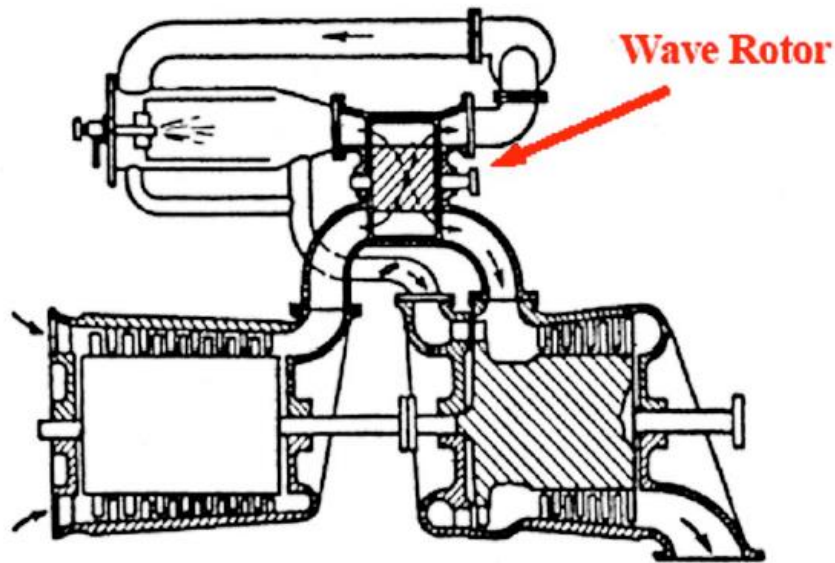


Fig 1.3.1 Wave rotor as a topping stage for the locomotive gas turbine

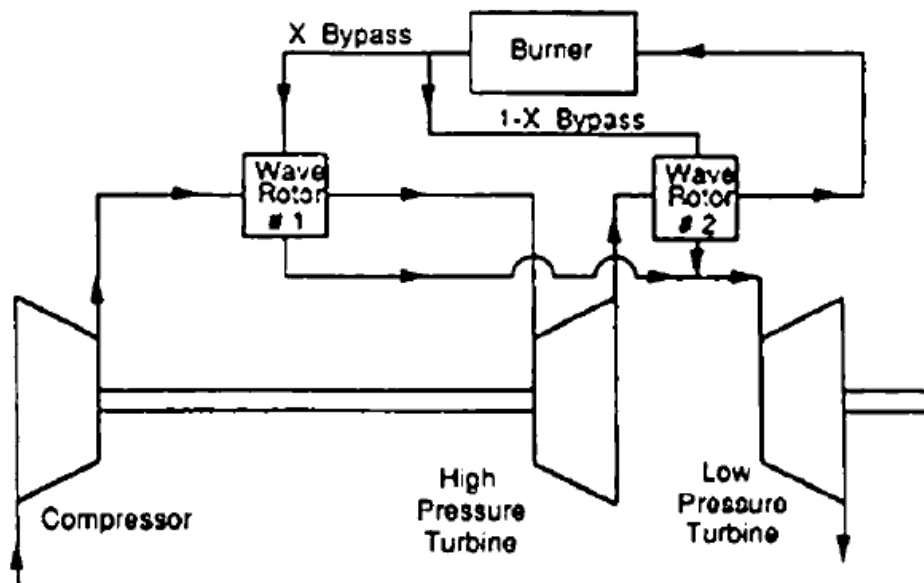
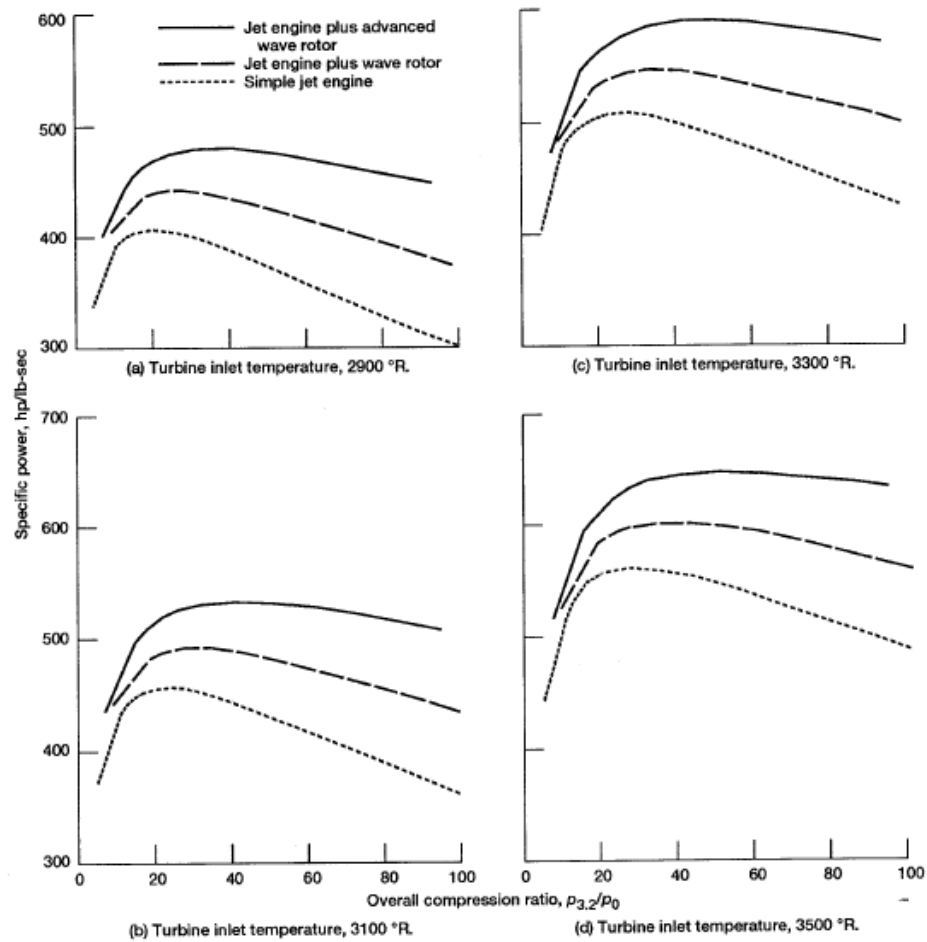


Fig 1.3.2 Schematic of a double wave rotor cycle

Due to its great potential in improving the performance of fluid machinery and energy utilizing. Since 1990s, NASA began the research on wave rotor. Among them, Wilson and Paxson^[14] published a feasibility study for topping jet engines with wave rotors which shown that a wave-rotor topped engine could have a better efficiency and power comparing with a simple one. And Welch's team^[15] also predict the benefits like

power improvement and fuel consumption decreasing by using wave rotor. In further study, NASA's teams improved the one-dimensional model according to the experimental data and use it to evaluate dynamic behavior, startup transients, and channel area variation, as preliminary design tool to optimize a four-port wave rotor



cycle for gas turbine topping. With the big investment, the research of wave rotors advanced by leaps and bounds at the time.

Fig 1.3.3 Paxson's study result about specific power

Recent years, with the improved methods, which the accurate simulation and experimental measurement techniques have a great development comparing to early stage, researchers could have a better configuration to improve the performance of wave rotor. Benefit from the popularization of technology, many universities also begin the academic research in wave rotor.

Michigan State University has conducted long-term research in many aspects on it since 2000s. P. Akbari's report^[16] has concluded many result including the topping cycle features, combination of QOD code with commercial software and so on.

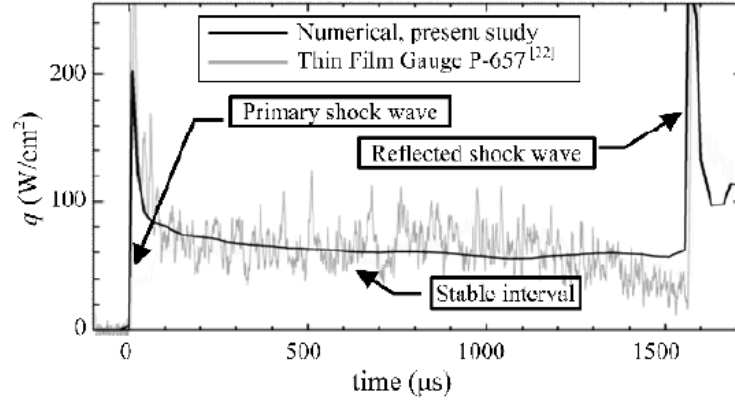


Fig 1.3.4 Time traces of unsteady heat flux at one point, from Okamoto

Okamoto and his team in University of Tokyo is another standard. Their research^[17] focusing on the thermal phenomenon in the wave rotor channel, validating the shock wave effect in heat transfer by model simulating and experiments. Also discuss the geometric effect and rotation factor in the research. The theory about the unsteady flow inside the channels are more and more completed.

1.4. Recent research and motivation

Nowadays, the research around wave rotor has gradually changed from improving efficiency and flow analysis to expanding use cases.

1.4.1 Wave Rotor unsteady flow research for design

Although the wave rotor study has been continued for a century, the unsteady flow inside the channel is still a focus. In early years, due to poor numerical study tool and measure methods, researchers conclude a model according to a large amount experiment and theoretical analysis data. Of course, it generally represents the feature of flow inside the wave rotor, while as we know, there is still a certain error due to the combination effect of turbulence, pressure wave and transfer behaviors. Thus, for

designing a wave rotor, the work becomes complex, even a prototype is produced, there is still a lot of experiments, calibration works need to be done. Also, the compatibility of wave rotor could be terrible due to that. Not to mention the other important technical problems like leakage.

Thanks to updated simulation tools and precise measure tools, the development of wave rotor is moving forward. Nowadays, a lot of researchers combine the numerical study and experimental to verify the consistency of them, which the feedback of the data would also be used to improve the numerical model. So far, the pressure wave, the viscosity effect and some other phenomenon could be simulated more precisely, which it further makes its promotion possible.

Besides, engineers try to find a generic way to design a wave rotor, such as *Iancu*^[41] has concluded some design steps, one of examples is shown in Fig 1.4.1.1. Also, we can define some parameters for wave rotor. Just like a design manual, these parameters could build a relationship at the data analysis level. If we need to design a wave rotor for a system, according to our requirement, we could fast get a series of available primary data, based on which it really supports a fast design method for engineers.

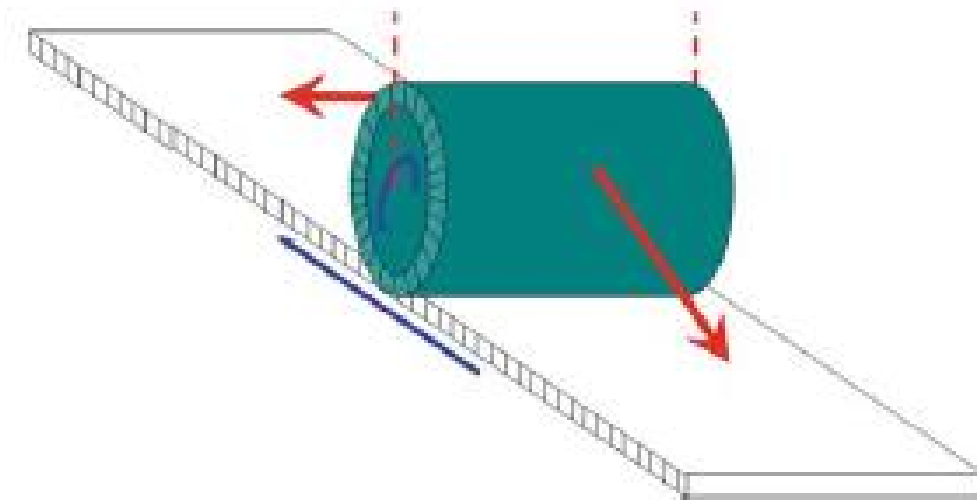


Fig 1.4.1.1 Example of design method: unfolding a 3D model as 2D objects

1.4.2 Wave Rotor Constant-Volume Combustor

Researchers are not satisfied with the wave rotor as a turbine or compressor, making systems compact is also a focus. The status quo in today's gas turbine engine is a nominal pressure-loss combustion process. Constant-volume combustion (CVC) systems that accomplish pressure gain have the potential to significantly cut fuel consumption and CO₂ emissions of gas turbines, power plants, and propulsion systems.

The wave rotor is a promising candidate for implementing CVC mechanically, delivering relatively steady outflow with low inherent losses and high durability. Previously used as dynamic pressure exchangers^{[18][19][20]} and considered as topping devices for gas turbine engines^{[21][22][23]}, wave rotors have been tested and reported as combustors in one prior test rig^[24]. Akbari and Nalim^{[25][26]} provide a detailed review of recent developments.

The wave rotor constant-volume combustor (WRCVC) utilizes unsteady wave motion and mechanical confinement to provide pressure gain during combustion. The combustion passages in a WRCVC are arrayed on the periphery of a drum that rotates between two stationary end plates, which house the intake and exit ports. Each passage is periodically charged and discharged as it rotates past partial-annular intake and exit ports located on end walls that function as the intake and exit valves. Premixed air-fuel mixtures flow sequentially, with possibly variable composition, into the rotating combustion passages as they become aligned with the intake port. The passages experience a substantial compression by a traveling shock process before combustion initiation, giving a thermodynamic advantage. When both ends close after charging, the mixture undergoes combustion at nominally constant volume when it is ignited, usually by a jet of hot gas at one or both ends (Fig. 1.4.2.1). Combustion must be completed before the passages rotate into alignment with the exit port, initiating the exhaust process. All wave rotors operate on the principle that optimal port location and rotation speed synchronizes valving at both ends and with internal non-steady processes. With a sufficiently large number of passages, there is relatively steady flow of accepted and

delivered gases, albeit with some spatial non-uniformity.

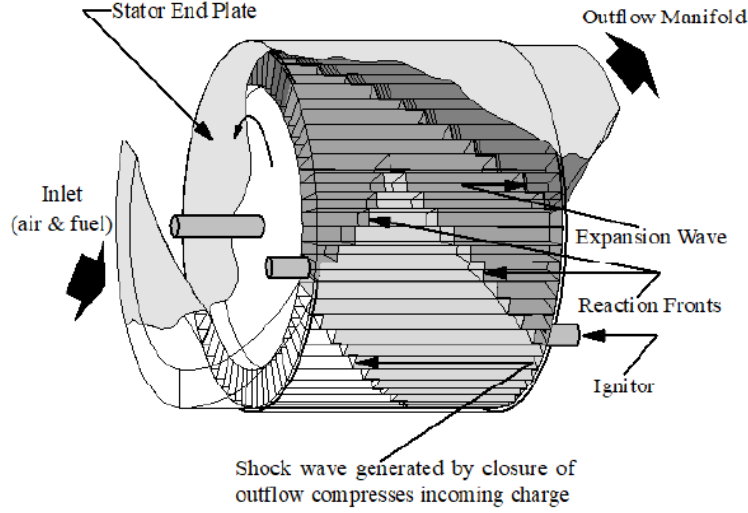


Fig 1.4.2.1 WRCVC schematic

Here we mainly introduce the transient gas-dynamic and combustion model. Design of the port locations and predictions of the flow field were made using a time-marching finite-volume model and numerical code, previously validated using pressure-exchange (non-combustion) wave rotor experiments^{[32][33][34]}. The initial model for design purposes used turbulence and reaction rate parameters based on prior WRCVC literature^{[27][28][29]} and turbulent combustion theory discussed below. The port geometry design^{[30][31]} based on the initial model was found acceptable after these parameters were refined through measurements. The interpretation of measurements presented below will be aided by first examining model predictions and validation. The time-marching, spatially one-dimensional model simulates the transient gas dynamics and combustion in one combustion passage of a WRCVC. Wave rotor operation is dominated by wave and flame propagation along the passages; thus variations in the other directions are considered negligible in the model. The code thus solves one-dimensional time-dependent mass, momentum, and energy equations together with equations for species or reaction progress variables, assuming uniform cross-section area and a calorically and thermally perfect gas with constant specific heat ratio (γ).

The source term(S) applicable to the internal region includes the effects of friction , heat transfer, turbulence and species conversion (combustion), and is given in Eq below. Leakage-related terms (radial and circumferential) were applied to the passage ends (terminal cells), but their complex details are omitted here for brevity.

$$S_{int} = \left[\begin{array}{c} 0 \\ \frac{\varepsilon_t}{Re} \frac{\partial^2 u}{\partial x^2} + \sigma_2 u |\rho u|^{0.75} \\ \frac{\varepsilon_t}{Re} \frac{\partial^2}{\partial x^2} \left(\frac{u^2}{2} + \frac{T}{(\gamma - 1) Pr_t} + \sum_{j=1}^n \frac{z_j q_j}{Sc_t} \right) + \sigma_3 u |\rho u|^{0.75} (T - T_w) \\ \frac{\varepsilon_t}{Re Sc_t} \frac{\partial^2 z_j}{\partial x^2} + \sum_{i=1}^m c_{ij} R_i \quad (j = 1, n - 1) \end{array} \right]$$

The numerical model validation is illustrated with two test runs of the origin which on-rotor combustion was successfully achieved, with different fuel distribution in the passage. The operation of WRCVC test rig and the dynamics of its operation are discussed in more detail in prior publications^{[35][36][37][38]}. Two test cases have the same targeted rotor speed, main air flow rate, ethylene fuel flow rate and torch igniter flow rate, which are all set in the simulation. The port boundary conditions are specified through an iterative process to match the flow rates of the simulations with that of the experiments, as there is no direct measure for the pressures and temperatures at the rotor interfaces. Finally, it is proved the consistency of simulation and experiment.

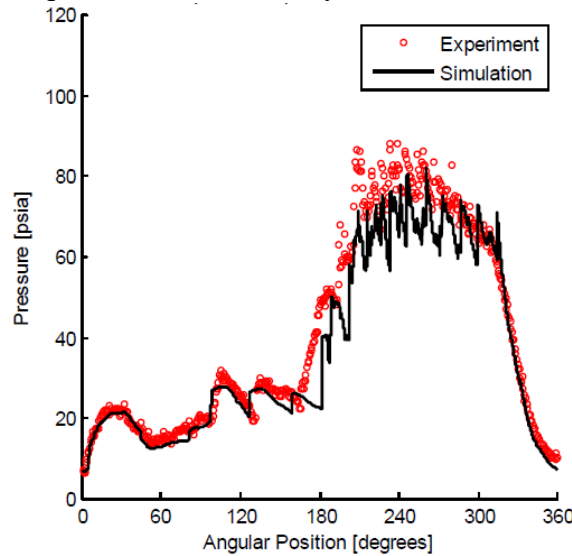


Fig 1.4.2.2 pressure plot comparison of wave rotor

1.4.3. Miniaturization

Miniaturization is a popular study direction for the whole mechanical industry. An example could be shown in robot industry. As the development of robots, the requirement of micro energy system is mentioned. Although the electrical energy has its advantages in size and efficiency, the problems of capacity still trouble the researchers. In this condition, thermal energy system becomes another possible source system for this requirement. Meanwhile, considering “high power mass ratio” is a feature for miniaturization, even micro plant needs an accessory system to improve its performance. Thus, the study of small wave rotor is also an available direction for researchers.

While the problems of miniaturization are always the same: the machines have to stand big stress and load with a small geometric size (like thin-walled structure). Apart from the mechanical stress, thermal stress is always a serious factor on it. With high operating temperature, the material will have a trend of expanding, the small strain inside material will lead to stress according to the elasticity. In other side, the high operating temperature also change the properties of material, make it weaker. More serious, it will directly damage the material structural, affect the life of machine or even destroy it (like creep).

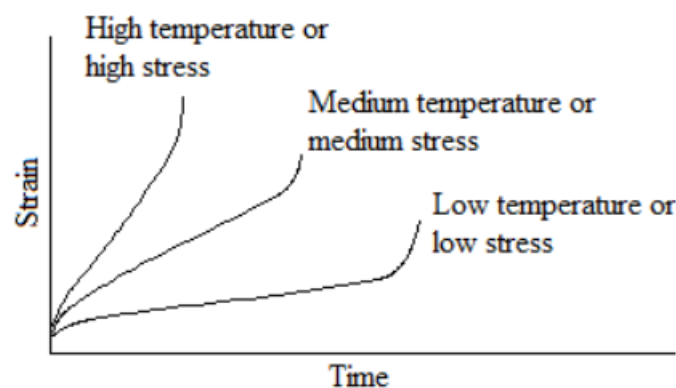


Fig 1.4.3.1 example of temperature effect in creep

1.4.4. Motivation

In fact, not only the high temperature effect will occur in the micro machine, but the big machine should also consider the problem as well. Especially, in the wave rotor, with period high temperature gas inject into the wave rotor channel, it's easy to increase the rotor's temperature in solid part. The high temperature gas will shock the wave rotor channel wall, lead to heat transfer between fluid and solid, which the behavior results to the enthalpy loss of the fluid and increase the solid temperature, meanwhile, the wall will also heat the fluid when fresh air come in. The cycle of temperature change would also lead to "alternating stress", affects the wave rotor's life.

For a better consideration when designing a wave rotor, it's meaningful to study the flow and thermal behaviors of wave rotors. The aim of this article is to do the aerothermal analysis for wave rotor. Base on the theoretical analysis, with numerical tools, building a proper model of wave rotor system. According to the simulation data, discuss the main factors influence to the flow properties, heat transfer behaviors and temperature distribution in the wave rotor.

2. Theoretical analysis

In this section, we will talk all the related behaviors in the wave rotor.

2.1. Topping cycle

The wave rotor could work as both a compressor and a turbine. In order to discuss the thermal process of the wave rotor cycle, the topping cycle is mentioned. Gas turbines are typical power sources used in a wide size range for propulsion and power generation systems. Recently, there has been considerable interest in the research, development, and application of small gas turbines yielding high power density and enabling low-cost air vehicles. However, resulting from the smaller size, their efficiency and pressure ratio, hence specific work, are mostly lower than those of the large-scale systems. Therefore, innovations are required to attractively enhance their performance.

At present, there are two major methods to enhance the performance of a simple cycle gas turbine:

- (1) improving the component efficiencies, especially of compressor and turbine.
- (2) improving the thermodynamic process of the cycle by increasing turbine inlet temperatures.

The aerodynamics of turbomachinery has already reached a very high level of component efficiencies up to around 90%. Still improvements are possible, but further huge enhancements seem to be unlikely. From a thermodynamic point of view, increasing the turbine inlet temperature is the most efficient way to improve both the overall efficiency and specific power. However, the maximum temperature of the gas entering the turbine is limited by material considerations. Thus, a considerable jump in performance of small gas turbines can only be achieved by applying advanced thermodynamic processes that are not subjected to this limitation. Topping a gas turbine with a wave rotor is an appropriate solution. The turbine inlet temperature may stay the

same while the combustion takes place at a higher temperature. Even, the turbine inlet temperature may be lowered. A pressure gains additional to that provided by the compressor is also obtained by the wave rotor. Therefore, the performance enhancement is achieved by increasing mostly both the overall efficiency and specific power, hence reducing the specific fuel consumption considerably. This occurs to be especially effective in the range of smaller gas turbines often used for propulsion of small vehicles or for distributed power generations.

To evaluate the performance enhancement of topping turbojet engines with wave rotors, a thermodynamic approach is used calculating the theoretic performance of wave-rotor-topped and baseline engines. The methodology is similar to the one introduced by Wilson and Paxson^[39] with some modifications.

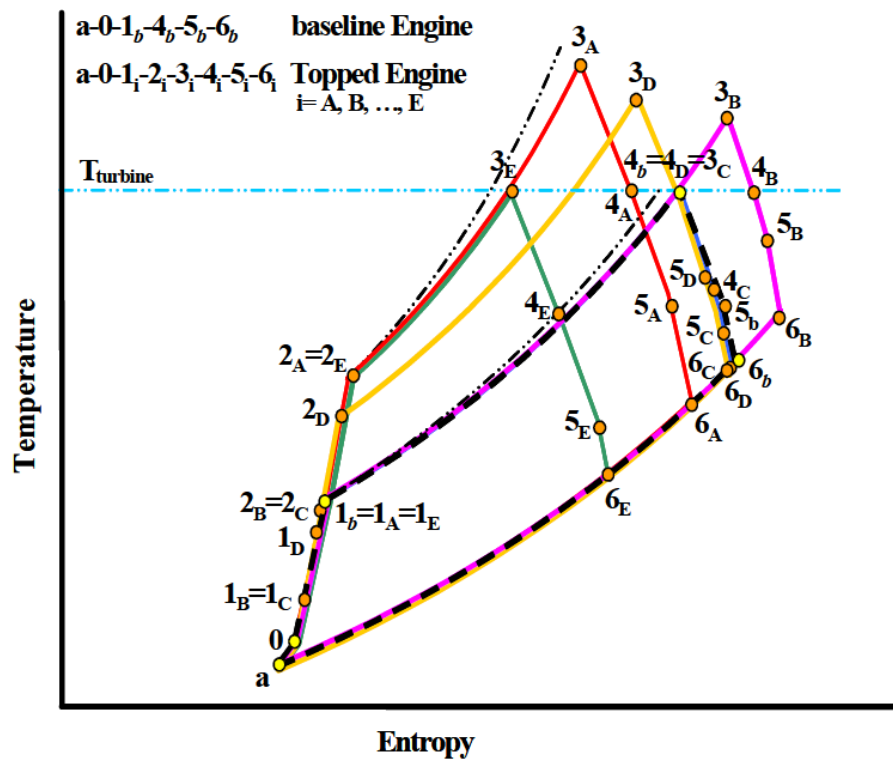


Figure 2.1.1 Schematic Temperature-Entropy diagram for a baseline cycle and five different wave-rotor-topped cycles

ANALYTICAL PROCEDURE^[40]

The following steps are followed to calculate the thermodynamic properties of the gases in different states of the topped cycle:

Path a-0:

With the given flight Mach number M , the stagnation temperature across the diffuser ($T_{ta}=T_{t0}$) is calculated by:

$$T_{t0} = T_{ta} = T_a \left(1 + \frac{\gamma_{air} - 1}{2} M^2 \right) \quad (1)$$

Using the definition of the diffuser isentropic efficiency (η_D), the diffuser outlet total pressure is obtained from:

$$\frac{P_{t0}}{P_a} = \left(1 + \eta_D \frac{u_a^2}{2 C_{p_{air}} T_a} \right)^{\gamma_{air} / \gamma_{air} - 1} \quad (2)$$

Path 0-1:

The compressor outlet total temperature and pressure are calculated by:

$$T_{t1} = T_{t0} + \frac{T_{t0}}{\eta_C} \left(R^{\frac{\gamma_{air}-1}{\gamma_{air}}} - 1 \right) \quad (3)$$

$$\frac{P_{t1}}{P_a} = \frac{P_{t1}}{P_{t0}} \frac{P_{t0}}{P_a} = R \cdot \frac{P_{t0}}{P_a} \quad (4)$$

where the compressor isentropic efficiency (η_C) relates the compressor pressure ratio (R) to the compressor polytropic efficiency (η_{pc}) through:

$$\eta_C = \frac{R^{\frac{\gamma_{air}-1}{\gamma_{air}}} - 1}{R^{\gamma_{air} \eta_{PC}} - 1} \quad (5)$$

Path 1-2:

The flow properties after the wave rotor compression process are obtained by:

$$T_{t2} = T_{t1} + \frac{T_{t1}}{\eta_{WC}} \left(PR_W^{\frac{\gamma_{air}-1}{\gamma_{air}}} - 1 \right) \quad (6)$$

$$\frac{P_{t2}}{P_a} = \frac{P_{t2}}{P_{t1}} \frac{P_{t1}}{P_a} = PR_W \cdot R \cdot \frac{P_{t0}}{P_a} \quad (7)$$

Path 2-3:

The fuel/air ratio ($f = m_f / m_{air}$) can be obtained by applying the energy equation to the combustion chamber as:

$$\eta_Q f h_{PR} = (1 + f) C_{p_{gas}} T_{t3} - C_{p_{air}} T_{t2} \quad (8)$$

where h_{PR} is the heating value of the fuel. The value of 43000 kJ/kg will be used for all calculations here. This equation gives f as:

$$f = \frac{C_{p_{gas}} T_{t3} - C_{p_{air}} T_{t2}}{\eta_Q h_{PR} - C_{p_{gas}} T_{t3}} \quad (9)$$

Alternatively, f can be expressed based on the turbine total inlet temperature (T_{t4}) and the compressor total exit temperature (T_{t1}). For this purpose, wave rotor compression and expansion specific works are defined respectively as follows:

$$w_{WC} = C_{p_{air}} (T_{t2} - T_{t1}) \quad (10)$$

$$w_{WE} = (1 + f) C_{p_{gas}} (T_{t3} - T_{t4}) \quad (11)$$

Here, it is justified that $m_1 = m_2 = m_{air}$ and $m_3 = m_4 = m_{air} + m_f$ (generally, the mass flow rates m_1 and m_2 are not quite the same. Similarly, mass flow rates m_3 and m_4 are not equal either). Now, Eq. (8) can be expressed as:

$$\eta_Q f h_{PR} = (1 + f) C_{p_{gas}} T_{t4} + w_{WE} - w_{WC} - C_{p_{air}} T_{t1} \quad (12)$$

since the net output work of the wave rotor is zero ($w_{wc} = w_{we}$), solving for f leads

$$f = \frac{Cp_{gas} T_{t4} - Cp_{air} T_{t1}}{\eta_Q h_{PR} - Cp_{gas} T_{t4}} \quad (13)$$

to:

For Cases C and E where T_{t3} is equal to the baseline inlet turbine temperature, Eq. (9) is used to calculate f . For Cases A, B, and D where T_{t4} is a known value and is equal to the baseline inlet turbine temperature, f can be obtained by using Eq. (13).

The relation between T_{t3} and T_{t4} can be found by equating Eq. (10) with (11):

Finally, the total pressure after the combustion chamber is obtained by:

$$\frac{P_{t3}}{P_a} = \frac{P_{t3}}{P_{t2}} \frac{P_{t2}}{P_a} = \Pi_{comb} \cdot PR_W \cdot R \cdot \frac{P_{t0}}{P_a} \quad (15)$$

Path 3-4:

To obtain the turbine inlet total pressure (p_{t4}), it is convenient to express the wave rotor compression and expansion works in terms of pressure ratios as follows:

$$\dot{W}_{WC} = \dot{m}_{air} Cp_{air} (T_{t2} - T_{t1}) = \frac{\dot{m}_{air} Cp_{air}}{\eta_{WC}} \left(PR_W^{\frac{\gamma_{air}-1}{\gamma_{air}}} - 1 \right) \quad (16)$$

$$\begin{aligned} \dot{W}_{WE} &= (\dot{m}_{air} + \dot{m}_f) Cp_{gas} (T_{t3} - T_{t4}) \\ &= (\dot{m}_{air} + \dot{m}_f) Cp_{gas} \eta_{WE} T_{t3} \left[1 - \left(\frac{P_0}{\eta_{comb} PR_W} \right)^{\frac{\gamma_{gas}-1}{\gamma_{gas}}} \right] \end{aligned} \quad (17)$$

where $P_0 = p_{t4}/p_{t1}$ is the gain pressure ratio across the wave rotor. Equating the compression work to the expansion work leads to:

$$\frac{Cp_{air} T_{t1}}{\eta_{WC}} \left(PR_W^{\frac{\gamma_{air}-1}{\gamma_{air}}} - 1 \right) = (1+f) Cp_{gas} \eta_{WE} T_{t3} \left[1 - \left(\frac{PO}{\eta_{comb} PR_W} \right)^{\gamma_{gas}-1/\gamma_{gas}} \right] \quad (18)$$

Substituting T_{t3} from Eq. (14) in the above equation and some algebra gives:

$$PO = \Pi_{comb} PR_W \left\{ 1 - \frac{A \frac{1}{\eta_{WE} \eta_{WC}} B}{1 + A \frac{1}{\eta_{WC}} B} \right\}^{\gamma_{gas}/\gamma_{gas}-1} \quad (19)$$

where

$$A = \frac{Cp_{air}}{(1+f) Cp_{gas}} \quad (20)$$

$$B = \frac{T_{t1}}{T_{t4}} \left[PR_W^{(\gamma_{air}-1)/\gamma_{air}} - 1 \right] \quad (21)$$

Equation (19) is a modified version of the “wave-rotor characteristic” equation introduced in the literature. This equation represents the performance of the wave rotor. By using Eq. (19), the turbine inlet total pressure is obtained by:

$$\frac{P_{t4}}{P_a} = \frac{P_{t4}}{P_{t1}} \frac{P_{t1}}{P_a} = PO \cdot R \cdot \frac{P_{t0}}{P_a} \quad (22)$$

Path 4-5:

In turbojet engines, by considering the mechanical transmission efficiency, the

$$Cp_{air} (T_{t1} - T_{t0}) = \eta_M (1+f) Cp_{gas} (T_{t4} - T_{t5}) \quad (23)$$

compressor shaft work equals the turbine output work:

Therefore, the total temperature of the gas leaving the turbine can be calculated as:

$$T_{t5} = T_{t4} - \frac{Cp_{air} (T_{t1} - T_{t0})}{\eta_M (1+f) Cp_{gas}} \quad (24)$$

To find the total pressure of the gas leaving the turbine (p_{t5}), the value of the turbine isentropic efficiency (η_T) is needed. There are two ways to calculate η_T for a turbine:

$$\eta_T = \frac{\left(\frac{p_{t5}}{p_{t4}}\right)^{(\gamma_{gas}-1)\eta_{PT}/\gamma_{gas}} - 1}{\left(\frac{p_{t5}}{p_{t4}}\right)^{\gamma_{gas}-1/\gamma_{gas}} - 1} \quad (25)$$

and

$$\eta_T = \frac{\left(\frac{T_{t5}}{T_{t4}}\right) - 1}{\left(\frac{p_{t5}}{p_{t4}}\right)^{\gamma_{gas}-1/\gamma_{gas}} - 1} \quad (26)$$

It is preferred to use the turbine polytropic efficiency η_{PT} to obtain p_{t5} . Therefore, by equating the above two equations:

$$\frac{p_{t5}}{p_{t4}} = \left(\frac{T_{t5}}{T_{t4}}\right)^{\frac{\gamma_{gas}}{(\gamma_{gas}-1)\eta_{PT}}} \quad (27)$$

or,

$$\frac{p_{t5}}{p_a} = \frac{p_{t4}}{p_a} \left(\frac{T_{t5}}{T_{t4}}\right)^{\frac{\gamma_{gas}}{(\gamma_{gas}-1)\eta_{PT}}} \quad (28)$$

Path 5-6:

For a given local pressure ratio at the nozzle exit (p_6/p_a), it is true that:

$$\frac{p_{t5}}{p_6} = \frac{p_{t4}}{p_a} \frac{p_{t5}}{p_{t4}} \frac{p_a}{p_6} = \frac{p_{t4}}{p_a} \frac{p_{t5}}{p_{t4}} \frac{1}{p_6/p_a} \quad (29)$$

Parameter p_{t5}/p_6 is a useful term to calculate the local gas temperature leaving the nozzle (T_6) by using the definition of the nozzle isentropic efficiency (η_N):

Since $T_{t5}=T_{t6}$, the nozzle exit velocity (u_6) can be calculated from:

$$u_6 = \sqrt{2Cp_{gas}(T_{t5} - T_6)} \quad (31)$$

$$T_6 = T_{t5} \left(\frac{1}{1 + \frac{\gamma_{gas}-1}{2} M_6^2} \right)^{\frac{\gamma_{gas}}{\gamma_{gas}-1}} \quad (32)$$

$$M_6 = \frac{u_6}{\sqrt{\gamma_{gas} R_{gas} T_6}}$$

Therefore, the nozzle exit Mach number is obtained by:

Finally, for the given p_6/p_a , the ratio of p_{t6}/p_a is calculated by:

After calculating the thermodynamic properties of all states in the cycle, it is possible to calculate the engine performance parameters.

$$T = (\dot{m}_{air} + \dot{m}_f) u_6 - \dot{m}_{air} u_a + (p_6 - p_a) A_N \quad (34)$$

The thrust produced by the engine is:

where A_N is the exhaust area of the nozzle. The pressure term $(p_6 - p_a) A_N$ is not zero only if the exhaust jet is supersonic. The specific thrust (thrust per unit mass flow of air) can be written as:

The pressure term can be presented as:

$$ST = (1 + f) u_6 - u_a + (p_6 - p_a) \frac{A_N}{\dot{m}_{air}} \quad (35)$$

$$(p_6 - p_a) \frac{A_N}{\dot{m}_{air}} = a_a \left[(1 + f) \frac{R_{gas}}{R_{air}} \frac{T_6/T_a}{u_6/a_a} \frac{1 - p_a/p_6}{\gamma_{air}} \right] \quad (36)$$

$$ST = (1 + f) u_6 - u_a + a_a \left[(1 + f) \frac{R_{gas}}{R_{air}} \frac{T_6/T_a}{u_6/a_a} \frac{1 - p_a/p_6}{\gamma_{air}} \right] \quad (37)$$

where a_a is the sound velocity of the entering air. Therefore, the specific thrust can be shown as:

Thus, the specific fuel consumption (SFC) can be simply obtained as:

Finally, the overall efficiency can be calculated by

$$\eta_o = \frac{ST u_a}{f h_{PR}} \quad (39)$$

2.2. Shock wave

An important phenomenon during pressure exchange process inside the wave rotor is shock wave or called pressure wave. The shock wave relations^[41] in two sides of wave could be generated as follows:

$$\Pi_S = \frac{p_2}{p_1} \quad (1)$$

$$\frac{T_2}{T_1} = \Pi_S \left(\frac{\frac{\gamma+1}{\gamma-1} + \Pi_S}{1 + \frac{\gamma+1}{\gamma-1} \Pi_S} \right) \quad (2)$$

$$w = a_1 \sqrt{\frac{\gamma+1}{2\gamma} (\Pi_S - 1) + 1} \quad (3)$$

$$u_p = \frac{a_1}{\gamma} (\Pi_S - 1) \sqrt{\frac{\frac{2\gamma}{\gamma+1}}{\Pi_S + \frac{\gamma-1}{\gamma+1}}} \quad (4)$$

Expansion wave relations^[41]:

$$\frac{a_2}{a_1} = 1 \pm \frac{\gamma-1}{2} \frac{u_2 - u_1}{a_1} \quad (5)$$

$$\frac{T_2}{T_1} = \left(\frac{a_2}{a_1} \right)^2 \quad (6)$$

$$\frac{p_2}{p_1} = \left(\frac{a_2}{a_1} \right)^{\frac{2\gamma}{\gamma-1}} \quad (7)$$

$$\begin{cases} u_{\text{head}} = a_1 \pm u_1 \\ u_{\text{tail}} = a_2 \pm u_2 \end{cases} \quad (8)$$

where the \pm sign represents the direction of the flow with respect to the direction of the wave.

Isentropic speed of sound:

$$a = \sqrt{\gamma R T} \quad (9)$$

Isentropic relation between total and static parameters:

$$\frac{T_0}{T} = 1 + \frac{\gamma - 1}{2} M^2 \quad (10)$$

$$\frac{p_0}{p} = \left(1 + \frac{\gamma - 1}{2} M^2 \right)^{\frac{\gamma}{\gamma - 1}} \quad (11)$$

2.3. Conservation law

There are three conservation equations to describe the physical balance of the item:

1. conservation of mass (so called continuity equation);
2. conservation of momentum (so called motion equation);
3. conservation of energy (from the first law of thermodynamics).

These three conservation equations are the basic of numerical analysis.

Let's consider a certain control volume dV with mass enter and exit.

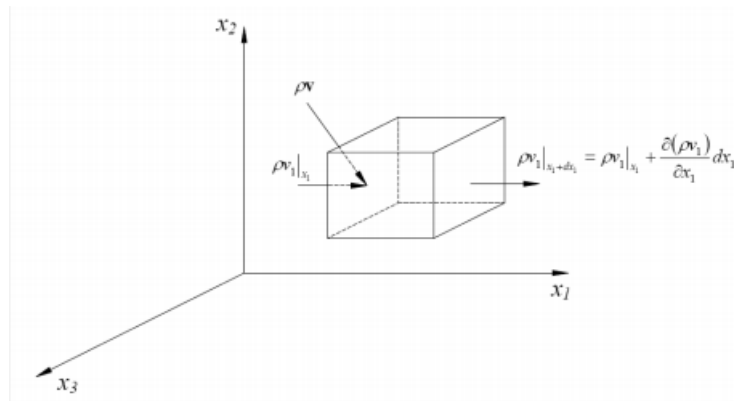


Fig 2.3.1 the scheme of mass conservation

The mass flow rate entering in the left face of dV is

$$\rho v_1|_{x_1} dx_2 dx_3$$

Similarly, the mass flow rate exiting in the right side:

$$\rho v_1|_{x_1+dx_1} dx_2 dx_3$$

Considering the dimensions of volume are infinitesimal, so it could use the Taylor expansion:

$$\rho v_1|_{x_1+dx_1} = \rho v_1|_{x_1} + \frac{\partial(\rho v_1)}{\partial x_1} dx_1$$

Meanwhile, we can generate the relation in other two directions and finally, using the divergence operator, we have the mass conservation equation:

$$\frac{\partial \rho}{\partial t} = -\nabla \cdot \rho \mathbf{v}$$

Then, let's consider the momentum equation, the scheme is shown below.

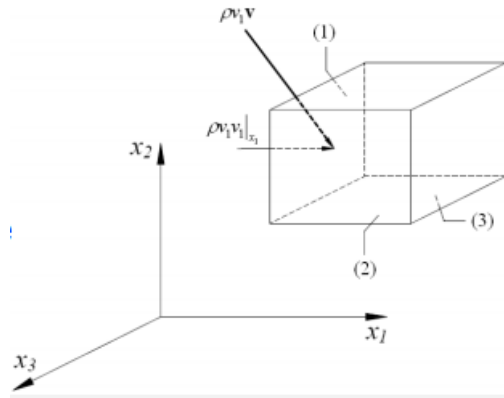


Fig 2.3.2 scheme of momentum conservation

Deriving from the mass conservation, the momentum conservation will have the similar form and it could be represented as:

$$\text{Rate of change of momentum} = \text{Net rate of momentum due to convection} + \text{external forces}$$

The flow entering the control volume brings the momentum of ρv , so the momentum flux entering the control volume:

$$v_1 \rho v dx_2 dx_3$$

$$-(\nabla \cdot \rho \mathbf{v} \mathbf{v}) dV$$

Thus, the net momentum flux is:

Considering the external forces terms, usually, we consider surface forces and gravity for common situations.

The surface forces are defined as stress tensor:

$$\boldsymbol{\sigma} = p\mathbf{I} + \boldsymbol{\tau}$$

Where, p is the pressure and $\boldsymbol{\tau}$ represents the viscosity stress.

In the case of Newtonian fluid, we have

$$\boldsymbol{\tau} = -\mu(\nabla\mathbf{v} + \nabla\mathbf{v}^T) + \left(\frac{2}{3}\mu - \kappa\right)(\nabla \cdot \mathbf{v})\mathbf{I}$$

By using divergence operator, the surface forces acting on control surface is:

The gravity is similar, so we can get the final momentum equation as follow,

$$\frac{\partial \rho \mathbf{v}}{\partial t} = -\nabla \cdot \rho \mathbf{v} \mathbf{v} - \nabla p - \nabla \cdot \boldsymbol{\tau} + \rho \mathbf{g}$$

And by using substantial derivative, the momentum equation becomes Navier-

$$\rho \frac{D\mathbf{v}}{Dt} = -\nabla p + \mu \nabla^2 \mathbf{v} + \rho \mathbf{g}$$

Stokes equation:

Considering the energy conservation, there would have more terms in the equation:

$$\begin{aligned} \text{Rate of change of the total energy} &= \text{net convective flow rate of the total energy} + \text{net heat flux} \\ &+ \text{rate of work done by pressure} \\ &+ \text{rate of work done by viscous stresses} \\ &+ \text{rate of work done by gravity} \end{aligned}$$

We can divide total energy to the internal energy and kinetic energy:

$$e = u + \frac{1}{2} \mathbf{v}^2 \equiv u + \frac{1}{2} \mathbf{v} \cdot \mathbf{v}$$

Then the rate of change of total energy is

$$\frac{\partial}{\partial t} \left(\rho u + \frac{1}{2} \rho \mathbf{v}^2 \right) dV$$

Net convective flow rate of the total energy is

$$-\nabla \cdot (\rho e \mathbf{v}) dV$$

Net heat flux is

$$-\nabla \cdot \mathbf{q} dV$$

Rate of work done by pressure:

$$-\nabla \cdot p \mathbf{v} dV$$

Rate of work done by viscous stresses

$$-\nabla \cdot (\boldsymbol{\tau} \cdot \mathbf{v}) dV$$

$$\rho \mathbf{g} \cdot \mathbf{v} dV$$

Rate of work done by gravity

We can get the energy conservation equation:

$$\frac{\partial}{\partial t} \left(\rho u + \frac{1}{2} \rho v^2 \right) = -\nabla \cdot \left(\left(\rho u + \frac{1}{2} \rho v^2 \right) \mathbf{v} \right) - \nabla \cdot \mathbf{q} dV - \nabla \cdot p \mathbf{v} - \nabla \cdot (\boldsymbol{\tau} \cdot \mathbf{v}) + \rho \mathbf{g} \cdot \mathbf{v}$$

If we use substantial derivative the energy equation could be

$$\rho \frac{Du}{Dt} = -\nabla \cdot \mathbf{q} - p \nabla \cdot \mathbf{v} - \boldsymbol{\tau} : \nabla \mathbf{v}$$

Let's introduce the definition of thermal expansion coefficient and specific heat:

$$\beta \doteq -\frac{1}{\rho} \left(\frac{\partial \rho}{\partial T} \right)_p$$

$$c_p = \left(\frac{\partial h}{\partial T} \right)_p$$

We can rewrite the energy equation as

$$\rho c_p \frac{DT}{Dt} = \nabla \cdot (k \nabla T) - \boldsymbol{\tau} : \nabla \mathbf{v} + \beta T \frac{Dp}{Dt}$$

After we deriving all the three equations, we can simplify them according to the model, such as if we consider the rigid solid, the velocity would be zero, or if we consider an steady state problem, the time derivative item would be zero.

Besides, there are some boundary conditions we need to set, for example,

For solid boundary:

1. for no-slip wall conditions

$$\mathbf{v} = \mathbf{v}_{wall}$$

2. Dirichelet boundary conditions (constant temperature)

$$T = T_{wall}$$

3. Neumann boundary conditions (conduction or adiabat, sometimes, the source term and radiation terms should be considered)

$$-k \nabla T \cdot \mathbf{n} = q_{wall}$$

4. Robin boundary conditions (convection)

For fluid boundary:

$$-k\nabla T \cdot \mathbf{n}|_{wall} = h(T - T_{\infty})$$
$$v = v_{inlet}$$

1. Velocity inlet (or outlet)

2. Pressure inlet (or outlet)

$$p = p_{outlet}$$

$$T = T_{inlet}$$

3. Fluid temperature (for inlet)

4. Convective flow (for outlet)

$$\partial T / \partial n = 0$$

2.4. Boundary layer theory

When the fluid flow through a plane, there would be a layer inside which the properties of fluid would be different, this is so called boundary layer. According to boundary layer theory^[42], along the vertical direction, the flow velocity will vary from zero to “ u ” which is called free stream velocity. The thickness of layer, strictly speaking, is an arbitrary value which is influenced by friction force. So, in near wall region, the viscosity has the main effect while in the far region, the interaction of molecular would be gradually decrease and be nil at infinity.

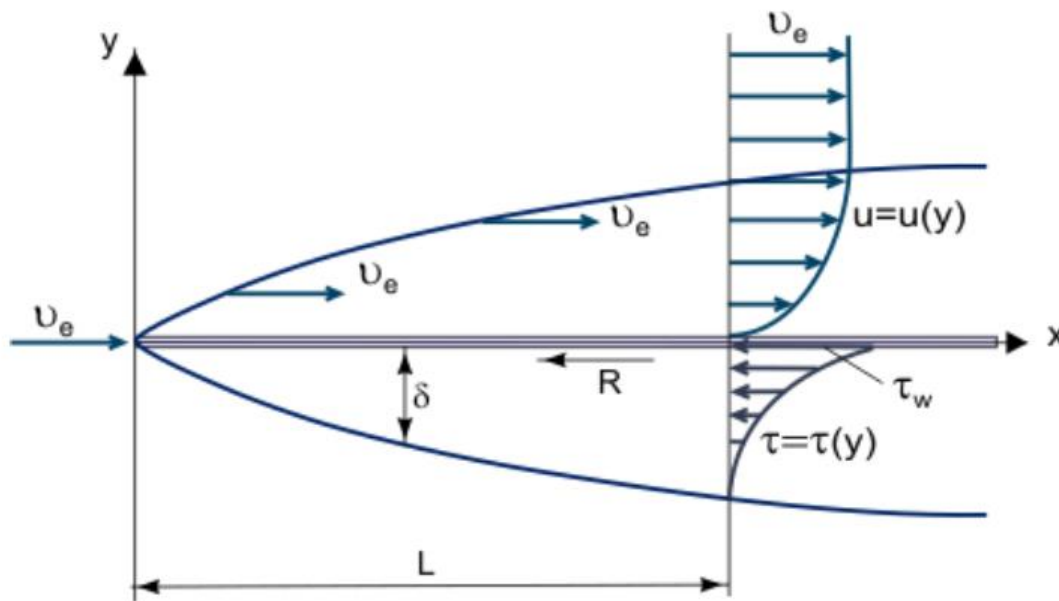


Fig 2.4.1 Boundary layer on a flat plate

An important number to describe the flow feature is Reynolds number which represents the ratio between inertial force and viscosity force. Especially, in the channel flow, with high Reynolds number, the viscosity force near the wall would be large due to high velocity change rate even the fluid has a low viscosity.

It is possible to ignore friction forces outside the boundary layer (as compared with inertia forces) to consider two flow regions: the boundary layer where friction effects are large and the almost Inviscid Flow core. On the premises that the boundary layer is a very thin layer ($\delta \ll L$, where L is the characteristic linear dimension of the body

over which the flow occurs or the channel containing the flow, its thickness decreasing with growth of Re), one can estimate the order of magnitude of the boundary layer thickness from the following relationship:

$$\delta/L = Re^{-0.5}$$

As was experimentally established, a laminar boundary layer develops at the inlet section of the body. Gradually, under the influence of some destabilizing factors, the boundary layer becomes unstable and transition of boundary layer to a Turbulent Flow regime takes place. Special experimental investigations have established the existence of a transition region between the turbulent and laminar regions. In some cases (for example, at high turbulence level of the external flow), the boundary layer becomes turbulent immediately downstream of the stagnation point of the flow. Under some conditions, such as a severe pressure drop, an inverse phenomenon takes place in accelerating turbulent flows, namely flow relaminarization.

Although its relative thinness, the boundary layer is very important for initiating processes of dynamic interaction between the flow and the body. The boundary layer determines the aerodynamic drag and lift of the flying vehicle, or the energy loss for fluid flow in channels (in this case, a hydrodynamic boundary layer because there is also a thermal boundary layer which determines the thermodynamic interaction of heat transfer).

Let's consider the 2D Navier–Stokes equations:

$$\begin{aligned}\frac{\partial u}{\partial x} + \frac{\partial v}{\partial y} &= 0 \\ u \frac{\partial u}{\partial x} + v \frac{\partial u}{\partial y} &= -\frac{1}{\rho} \frac{\partial p}{\partial x} + \nu \left(\frac{\partial^2 u}{\partial x^2} + \frac{\partial^2 u}{\partial y^2} \right) \\ u \frac{\partial v}{\partial x} + v \frac{\partial v}{\partial y} &= -\frac{1}{\rho} \frac{\partial p}{\partial y} + \nu \left(\frac{\partial^2 v}{\partial x^2} + \frac{\partial^2 v}{\partial y^2} \right)\end{aligned}$$

By using it in the boundary layer and ignoring the small term of y direction equation for laminar boundary layer, the last two equation becomes:

$$u \frac{\partial u}{\partial x} + v \frac{\partial u}{\partial y} = -\frac{1}{\rho} \frac{\partial p}{\partial x} + \nu \frac{\partial^2 u}{\partial y^2}$$

$$\frac{1}{\rho} \frac{\partial p}{\partial y} = 0$$

Due to that the wall is very thin and longitudinal pressure gradient could be considered as constant, then we can substitute the free stream velocity, we get:

$$u \frac{\partial u}{\partial x} + v \frac{\partial u}{\partial y} = U \frac{dU}{dx} + \nu \frac{\partial^2 u}{\partial y^2}$$

Now, with proper initial value, the partial differential equations could be solved.

Then, let's consider the convective constant. There is the relation:

$$\frac{v_x - v_S}{v_\infty - v_S} = \frac{v_x}{v_\infty} = \frac{v_y}{v_\infty} = 0 \quad \text{at} \quad y = 0$$

$$\frac{v_x - v_S}{v_\infty - v_S} = \frac{v_x}{v_\infty} = 1 \quad \text{at} \quad y = \infty \text{ and } x = 0$$

Where v_s is the moving wall speed, if we consider a stationary wall, it is nil.

Let's consider the Energy balance equation and mass balance equation in steady state, as shown below:

$$v_x \frac{\partial T}{\partial x} + v_y \frac{\partial T}{\partial y} = \frac{k}{\rho C_p} \frac{\partial^2 T}{\partial y^2}$$

$$v_x \frac{\partial c_A}{\partial x} + v_y \frac{\partial c_A}{\partial y} = D_{AB} \frac{\partial^2 c_A}{\partial y^2}$$

Substituting to preview equation, we have:

$$\frac{v_x - v_S}{v_\infty - v_S} = \frac{T - T_S}{T_\infty - T_S} = \frac{c_A - c_{AS}}{c_{A\infty} - c_{AS}} = 0 \quad \text{at} \quad y = 0$$

$$\frac{v_x - v_S}{v_\infty - v_S} = \frac{T - T_S}{T_\infty - T_S} = \frac{c_A - c_{AS}}{c_{A\infty} - c_{AS}} = 1 \quad \text{at} \quad y = \infty \text{ and } x = 0$$

According to experimental relation, we have the shear force

$$\tau_0 = \left(\frac{\partial v_x}{\partial y} \right)_{y=0} = 0.332 \frac{v_\infty}{x} Re^{1/2}$$

Also, according to the experiment equation, we can calculate:

$$\left(\frac{\partial T}{\partial y}\right)_{y=0} = 0.332 \frac{T_{\infty} - T_S}{x} Re^{1/2}$$
$$\left(\frac{\partial c_A}{\partial y}\right)_{y=0} = 0.332 \frac{c_{A\infty} - c_{AS}}{x} Re^{1/2}$$

We know that, in the flow, the main heat transfer method is convection, so we have

$$\frac{q}{A} = -k \left(\frac{\partial T}{\partial y}\right)_{y=0} = h_x (T_S - T_{\infty})$$

Then, we could get local convective heat transfer coefficient:

$$h_x = 0.332 \frac{k}{x} Re_x^{1/2} Pr^{1/3}$$

And similarly, we could generate the relationship of mass transfer in the boundary layer, and finally we get local convective mass transfer coefficient:

$$k'_x = 0.332 \frac{D_{AB}}{x} Re_x^{1/2} Sc^{1/3}$$

Where, Pr is Prandtl number and Sc is Schmidt number. Both of them are dimensionless constants

3. Model developing

After we have prepared all the numerical theories used in the analysis, we could begin to build the numerical model of the wave rotor now. In this article, the commercial CFD software Fluent and ANSYS R2020 are used.

3.1. Introduction of software

ANSYS software is a large-scale general FEA software developed by ANSYS Inc. It is the fastest growing CAE tool in the world which can interface with most CAD software. ANSYS has a wide application in nuclear industry, railways, petrochemicals, aerospace, machinery manufacturing, energy, automotive transportation, electronics, civil engineering, biomedicine, mining, water conservancy and home appliances.

ANSYS has a great kinds of sub-software packages for various kinds of numerical problems which includes:

1. Structural static analysis, used to solve the displacement, stress and force caused by external load. Static analysis is suitable for solving problems where the influence of inertia and damping on the structure is not significant. The static analysis in the ANSYS program can not only perform linear analysis, but also non-linear analysis, such as plasticity, creep, expansion, large deformation, large strain and contact analysis.
2. Structural dynamic analysis, used to solve the influence of time-varying loads on structures or components. Unlike static analysis, dynamic analysis considers the time-varying force load and its effect on damping and inertia. The types of structural dynamics analysis that ANSYS can perform the analysis like transient dynamics analysis, modal analysis, harmonic response analysis, and random vibration response analysis.
3. Thermal analysis, the program can handle three basic types of heat transfer: conduction, convection, and radiation. The three types of heat transfer can be

used for steady-state and transient, linear and nonlinear analysis. Thermal analysis also has the ability of phase change analysis that can simulate the process of material solidification and melting, and the ability to simulate the thermal-structure coupling analysis between heat and structural stress.

4. Fluid-dynamic analysis, the analysis type can be transient or steady. The result of the analysis can be the pressure at each node and the flow rate through each unit. And can use the post-processing function to produce a graphic display of pressure, flow rate and temperature distribution. In addition, three-dimensional surface effect units and heat-fluid tube units can be used to simulate the fluid flow around the structure and include convective heat transfer effects.
5. Acoustic analysis, used to study the propagation of sound waves in fluid-containing media, or to analyze the dynamic characteristics of solid structures immersed in fluids.
6. Electromagnetic field analysis, used for the analysis of electromagnetic field problems, such as inductance, capacitance, magnetic flux density, eddy current, electric field distribution, magnetic field line distribution, force, motion effect, circuit and energy loss, etc. It can also be used in the design and analysis of solenoids, regulators, generators, inverters, magnets, accelerators, electrolytic cells and non-destructive testing devices.

Besides, ANSYS support many pre-process modes, help the users building the geometric features and meshing the geometry for further simulation.

Fluent software uses the finite volume method based on a completely unstructured mesh, and has a gradient algorithm based on mesh nodes and mesh elements. It can achieve the steady/unsteady flow simulation and contains three algorithms: non-coupled implicit algorithm, coupled explicit algorithm, and coupled implicit algorithm, which support several choices for users.

Fluent also has powerful mesh support capabilities, supporting discontinuous mesh, hybrid mesh, dynamic/deformable mesh, sliding mesh and overset mesh. It is

worth emphasizing that Fluent software also has a variety of solution-based mesh adaptation and dynamic adaptation technologies, as well as technologies that combine dynamic mesh and mesh dynamic adaptation.

The most exceptional feature of Fluent is its rich and advanced turbulence models, allowing users to accurately simulate inviscid, laminar, and turbulent flows. Turbulence models include Spalart-Allmaras model, $k-\omega$ model group, $k-\epsilon$ model group, Reynolds stress model (RSM) group, large eddy simulation model (LES) group, and the latest separated eddy simulation (DES) and V2F models.

Besides, Fluent support many interfaces for users to realize many kinds of users define functions, such as TUI, GUI, UDF. Users could use C word to describe the function they want, by loading the c files, the Fluent could execute the code. By which users could solve more complex problems by using the basic frame.

3.2. 3D model building and meshing

Due to the fact that the analysis work is lack of the support by experiments, we try to borrow the data of Deng's study^[17] and, based on it, study the thermal behaviors of wave rotor. To simplify the problem, one channel of the wave rotor would be simulated.

According to the article, we can get the geometric feature of the wave rotor as shown in the Fig 3.2.1 and Table 3.2.1,

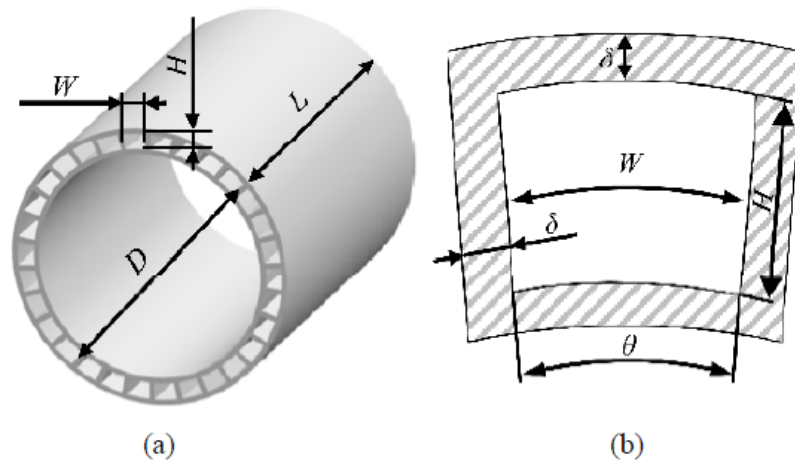


Fig 3.2.1 Geometric model of cell array of wave rotor (a); and cross section view of cell (b)

Table 3.2.1.

Midspan diameter	D	47	mm
Length	L	69	mm
Cell internal midspan width	W	3.92	mm
Cell internal height	H	3	mm
Cell internal degree	θ	9.6	°
Cell wall thickness (tang)	δ_t	1	mm
Cell wall thickness (radi)	δ_r	2	mm

Considering the TF connection, the position of half ports (symmetric) is shown in Fig 3.2.2:

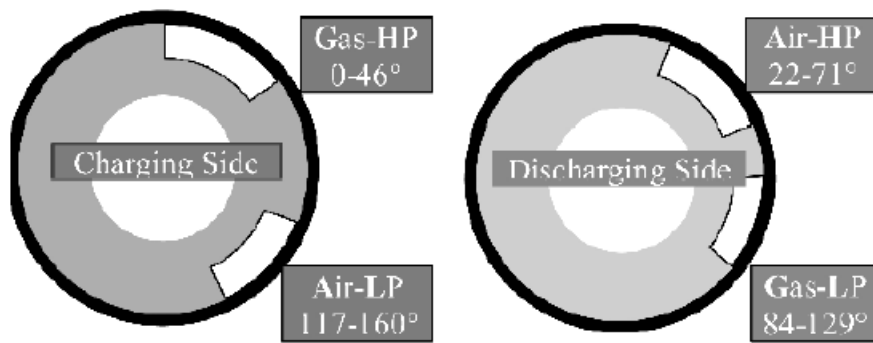


Fig 3.2.2 Port configurations of wave rotor with half part display

Consider only the fluid part with channel solid part, finally we can build the 3D model as shown below:

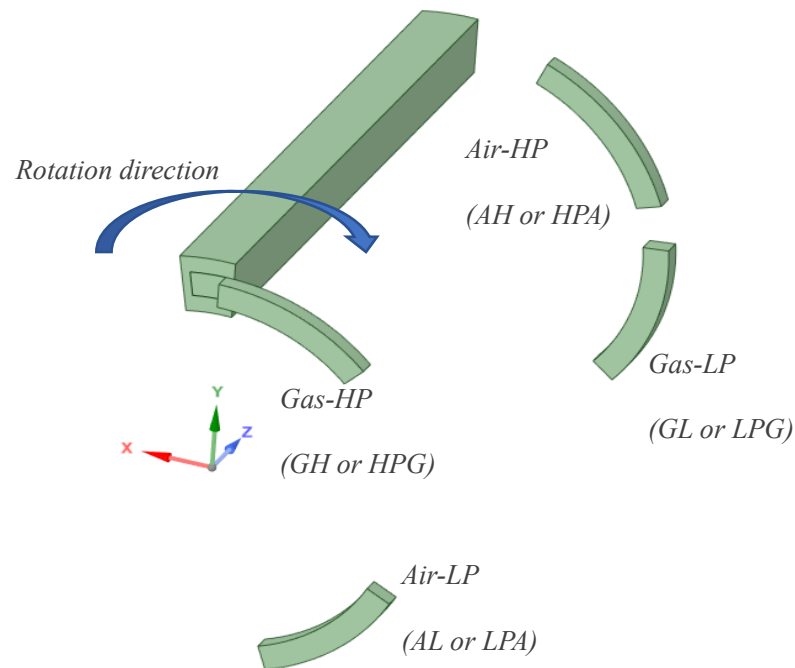


Fig 3.2.3 3D model of single channel wave rotor

3.3. Meshing

By using ANSYS Mesh mode, we can generally mesh the models.

3.3.1. Solid part meshing

Consider that the solid part is a rigid body, there is not deforming and structural destruction behaviors would happen. So, the solid parts mainly focus on the thermal transmission problems.

Define the part as “Solid”. Using “Multizone” method to mesh the part with prism mesh type, we can get a general uniform mesh result. According to the experience, there should be at least three mesh layers in one direction for making sure the precise of the thermal conduction calculation. Thus, finally, the element size of solid part is 0.0004 m, and it's displayed as Fig 3.3.1.1, own 234435 nodes and 82348 elements.

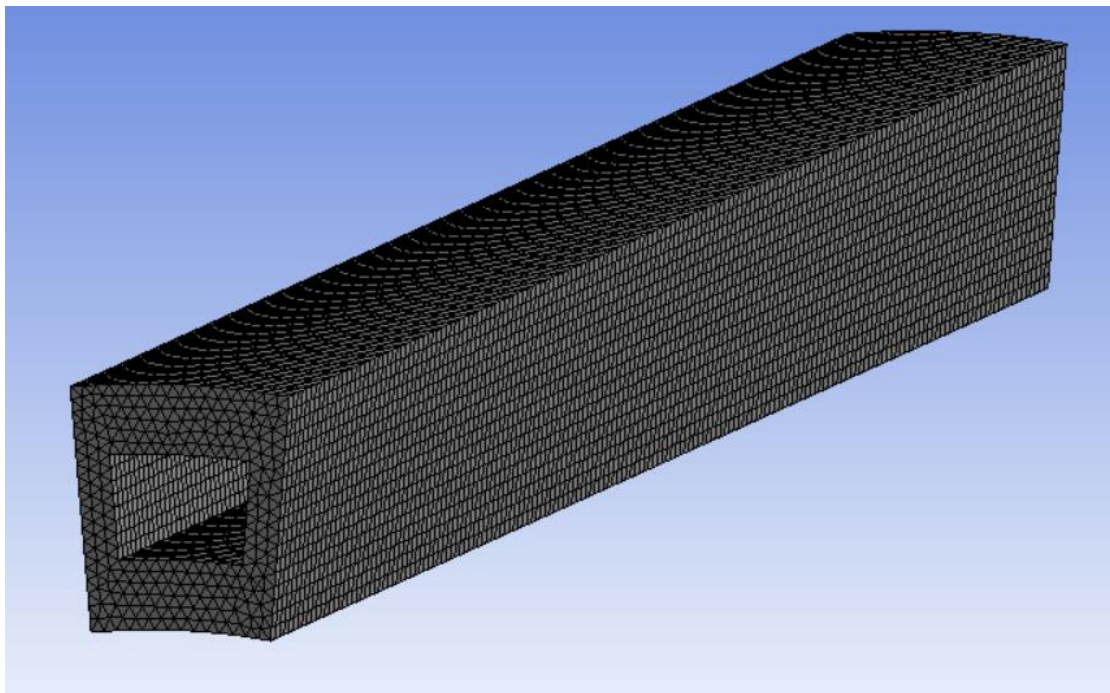


Fig 3.3.1.1 Mesh result of solid part

After meshing process, we need to name each surface of the part for further setting in fluent. (although we can do the same thing in the fluent, that's more complex to find the surface what we want due to several empty surfaces automatic created by fluent. Also, fluent will combine the similar surface, you have to divide them before setting)

3.3.2. Fluid part meshing

Consider that fact that, there is not local refining required in the solid part due to it's already a thin structural, the mesh size is small enough. The condition is more complex in the fluid part. With the moving channel, the wall of fluid part shall also be related to the shock. The near wall behavior wall strongly influences the heat transfer process. Thus, the local refinement or called boundary layer mesh is needed.

In order to obtain a proper value of layer mesh size, we need to consider its y^+ number^[44]. y^+ is a non-dimensional wall distance defined for determining the turbulence behavior in the law of the wall. y^+ could be calculated according to the equation:

$$y^+ = \frac{y u_\tau}{\nu}$$

Where, the y is the distance between calculation point and wall;

ν is the kinetic viscosity of fluid;

u_τ is called the friction velocity or shear velocity, calculated by

$$u_\tau = \sqrt{\frac{\tau_w}{\rho}}$$

τ_w is the wall shear stress;

ρ is the fluid density.

Also, we have dimensionless velocity as ratio of velocity and stress velocity:

$$u^+ = \frac{u}{u_\tau}$$

The law of the wall describes the relationship between two dimensionless parameters:

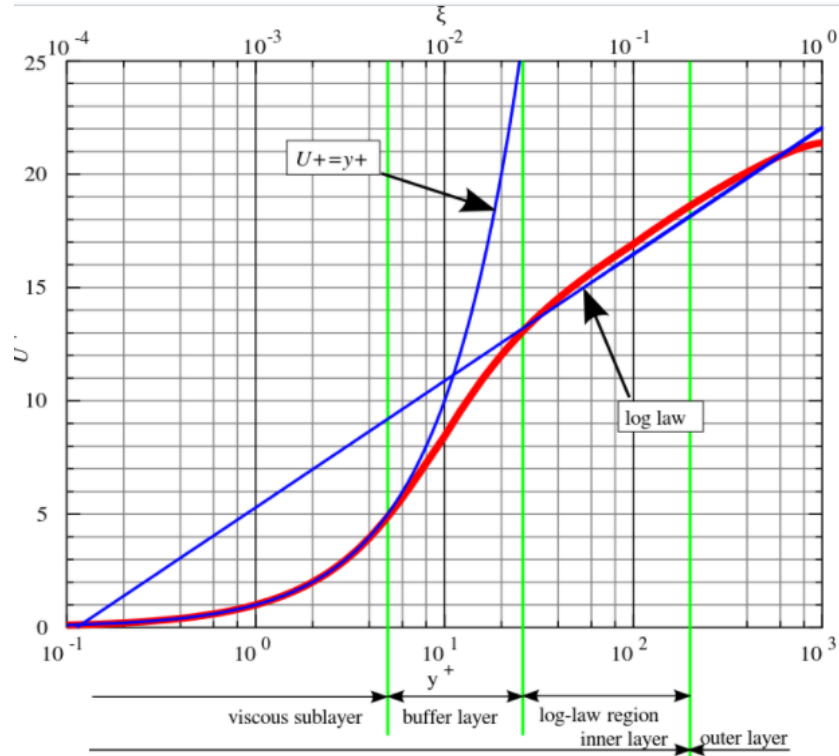


Fig 3.3.2.1 Relationship of y^+ and u^+

We can divide the relation inside the boundary layer as three stages. In the first stage called viscous sub-layer, y^+ number smaller than 5, the viscosity force domain the fluid region and the experimental equation is given as $y^+ = u^+$. In the second stage with y^+ larger than 5 and smaller than 30, both linear approach and log approach couldn't precisely predict the fluid feature, the max error occur in $y^+ = 11$, in two side of this critical value, linear approach and log approach are used. When y^+ number larger than 30, it follows the log law as:

$$u^+ = \frac{1}{\kappa} \ln y^+ + C^+$$

κ is Von Kármán constant, and C^+ is another experimental defined constant.

In wave rotor channel, with high Re number and high various unsteady flow which its max Mach number would be around 1, k- ϵ model is an available viscous model for numerical calculation, while it is only valid in the area of turbulence fully developed, and do not perform well in the area close to the wall. In order to deal with the near wall region, wall functions or called near wall treatment should be considered.

Wall functions equations are experimentally derived and used to satisfy the fluid relation in the near wall region. The first cell center needs to be placed in the log-law region to ensure the accuracy of the results. Wall functions are used to bridge the inner region between the wall and the turbulence fully developed region. When using the wall functions approach, there is no need to resolve the boundary layer causing a significant reduction of the mesh size and the computational domain.

A good number for first layer y^+ number is around 100. According to our case, using “ y^+ calculator”, we could know a proper size for first layer mesh is 0.0001 m. By using “inflation” function, we can set the boundary layer mesh. Consider the grow rate of size is 1.2 with 5 mesh layers, with also “Multizone” method and ‘Hexa’ mesh type. Finally, we can get a good mesh result as shown below:

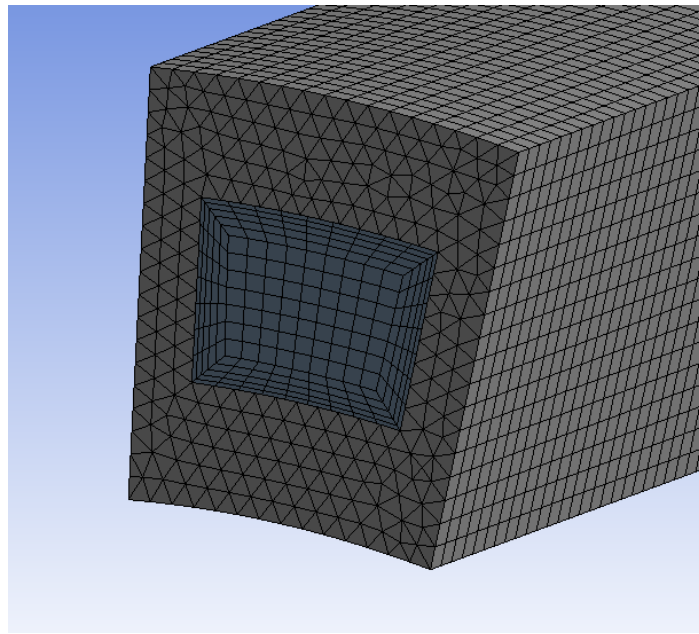


Fig 3.3.2.2 channel fluid mesh result with boundary layer mesh

After we finish the mesh work, similarly, we need to name the surface. The important thing is software will automatically set the contact region for model, while in the fluent, the contact region will form the interface, system automatically create the overlap surface and non-overlap surface. Considering the complex surfaces are, we choose to delete all the contact relation and they would be set later.

Besides, the global mesh size is set as 0.0005 m. We can use the built-in statistic tool to check the quality of mesh. For fluent calculation, quality of elements should better larger than 0.2, and the better the quality, the faster and precise it would be. According to the statistics, the qualities of elements are all larger than 0.5 as shown below:

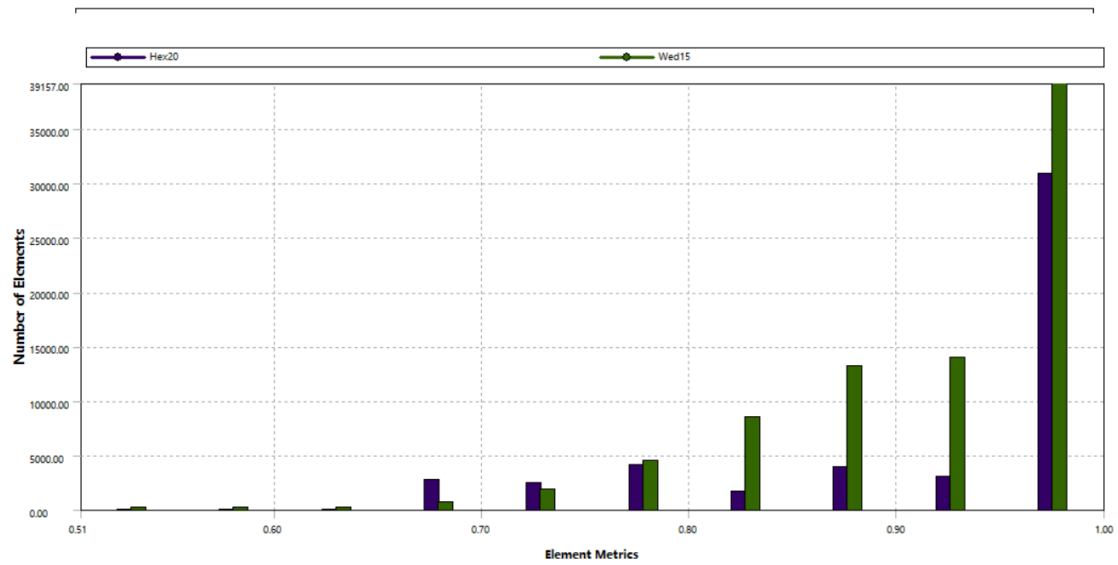


Fig 3.3.2.3 Statistics of element orthogonal quality

3.4. Model development in Fluent

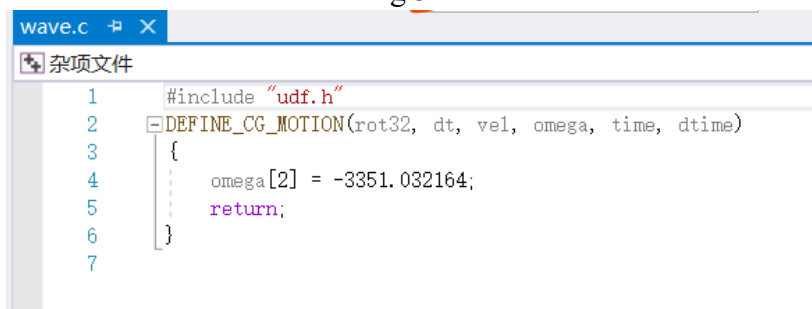
By reading the mesh file we export in Fluent, we can begin our next jobs. As we mentioned above, the numerical calculation requires the definition to the properties of materials and boundary condition of region boundaries. Also, the physical models, solvers and initial state should be discussed. Moreover, we should set the post-process tools like monitor, animations and UDF if necessary.

3.4.1. Dynamic mesh

To solve the moving body problems, Fluent support four possible methods:

1. Frame motion, it could be only used to solve the steady state problems by considering a reference coordinates motion. The calculation speed is faster than sliding mesh method, while, in some complex problems, the precision should be considered.
2. Sliding mesh, it could be used for both steady state and transient analysis. The data would be exchanged by interpolation in the sliding interface, the mesh would not be re-built, thus decrease the re-mesh time but the precision is not very good compare with dynamic mesh.
3. Dynamic mesh, usually used for transient analysis, when body moving, the mesh would be also deformed or re-meshed by system for precisely calculation.
4. Overset mesh, the overset mesh needs a background mesh and a moving mesh, used for transient problems. In the overset region, the two types of mesh will both calculate the result and exchange the data for improving the precision. The non-overlapping region would be calculated according to the background nodes. This method does not need re-mesh process, allow a more uniform mesh of models. It can calculate the problems faster with nice precision. However, it is not appropriate for complex geometry.

In our model, dynamic mesh method is chosen. The motion of the rotor is defined by UDF file. Consider all parts in model is rigid without deformation, we use “CG_MOTION” sentence as shown in Fig 3.4.1.1:



```
1  #include "udf.h"
2  DEFINE_CG_MOTION(rot32, dt, vel, omega, time, dttime)
3  {
4      omega[2] = -3351.032164;
5      return;
6  }
7
```

Fig 3.4.1.1 C code of UDF file used to define zone motion

It's written with C word, describe the kind of motion (“vel” = velocity, “omega” = rotation speed), the portion of three directions (“0” = X axis, “1” = Y axis, “2” = Z axis, “-” means reverse direction), and various of parameters according to time if necessary.

Although Fluent can change the unit of each parameters, once you load the UDF file, the physical quantity of defined parameters would be fixed. The default rotation speed unit is rad/s, in order to prevent the mistake, we set value of omega as rad/s which represents a rotation speed as 32000 rpm. Once we load the UDF file, we can define the motions of moving zones in dynamic mesh interface. Besides, there are three basic methods to change the mesh mentioned below and, in the model, layering method is used.

1. Smoothing, the concept of smoothing method is to use spring theory in the mesh element, with small deforming, the mesh would be extended or compressed. It's used for tetrahedron mesh.
2. Layering, used for hexahedron mesh, the concept is to delete and re-build the nodes in the zone motion and keeps shape of elements.
3. Remeshing, should be active with mesh smoothing, the concept is to re-mesh a part of neighborhood region when the mesh quality lower than a threshold.

3.4.2. Physical model and solver

Simulate the unsteady flow is a transient problem. Consider that the max Mach number is around 1, and the minimum fluid velocity (related to channel) is nearly 0, a pressure-based model would be proper. (Of course, for medium Mach number problem, pressure-based solver and density-based solver are both available, but the pressure-based solver has a greater compatibility).

Consider it is a high pressure and compressible fluid problem, the coupling algorithm should be chosen rather than SIMPLE or PISO for Pressure-Velocity calculation. And the properties of fluid are setting as follow. The density should be “ideal-gas” for compressible effect. The other parameters are kept as default in database.

Create/Edit Materials

Name: air

Material Type: fluid

Chemical Formula:

Fluent Fluid Materials: air

Mixture: none

Order Materials by: ☒ Name ☐ Chemical Formula

Fluent Database...
GRANTA EDS Database...
User-Defined Database...

Properties

Density (kg/m3): ideal-gas [Edit...]

Cp (Specific Heat) (j/kg-k): constant [Edit...]
1006.43

Thermal Conductivity (w/m-k): constant [Edit...]
0.0242

Viscosity (kg/m-s): constant [Edit...]
1.7894e-05

Molecular Weight (kg/kmol): constant [Edit...]
28.966

Change/Create Delete Close Help

Fig 3.4.2.1 Properties of fluid

Besides, the solid material is considered as Aluminum, the parameters keep default.

The screenshot shows the 'Create/Edit Materials' dialog box. The 'Name' field contains 'aluminum' and the 'Chemical Formula' field contains 'al'. The 'Material Type' is set to 'solid' and the 'Mixture' is set to 'none'. The 'Order Materials by' section has 'Name' selected. The 'Properties' section shows default values for Density (kg/m3) as 2719, Cp (Specific Heat) (j/kg-k) as 871, and Thermal Conductivity (w/m-k) as 202.4. The 'Change/Create' button is highlighted.

Fig 3.4.2.2 Properties of solid

Considering the physical model, according to our project, the Energy model should be activated. We choose k- ϵ model as turbulence model, which the model contains two equation to solve the turbulence phenomenon:

$$\frac{\partial(\rho k)}{\partial t} + \frac{\partial(\rho k u_i)}{\partial x_i} = \frac{\partial}{\partial x_j} \left[\frac{\mu_t}{\sigma_k} \frac{\partial k}{\partial x_j} \right] + 2\mu_t E_{ij} E_{ij} - \rho \epsilon$$

$$\frac{\partial(\rho \epsilon)}{\partial t} + \frac{\partial(\rho \epsilon u_i)}{\partial x_i} = \frac{\partial}{\partial x_j} \left[\frac{\mu_t}{\sigma_\epsilon} \frac{\partial \epsilon}{\partial x_j} \right] + C_{1\epsilon} \frac{\epsilon}{k} 2\mu_t E_{ij} E_{ij} - C_{2\epsilon} \rho \frac{\epsilon^2}{k}$$

Where, k is the turbulent kinetic energy and ϵ is the dissipation term.

Both of two equation could be generated as:

$$\begin{aligned} & \text{Rate of change of } k \text{ or } \epsilon + \text{Transport of } k \text{ or } \epsilon \text{ by advection} = \\ & \text{Transport of } k \text{ or } \epsilon \text{ by diffusion} + \text{Rate of production of } k \text{ or } \epsilon - \text{Rate of destruction of } k \text{ or } \epsilon \end{aligned}$$

According to ANSYS guidance, the realizable model is more appropriate for high Re condition. Besides, the near wall treatment or called wall function could be chosen as enhanced wall treatment, due to its great compatibility. What's more, the compressibility effect and viscous heating effect should be considered. The turbulence model configurations are shown below:

Viscous Model

Model

- ☐ Inviscid
- ☐ Laminar
- ☐ Spalart-Allmaras (1 eqn)
- ☒ k-epsilon (2 eqn)
- ☐ k-omega (2 eqn)
- ☐ Transition k-kl-omega (3 eqn)
- ☐ Transition SST (4 eqn)
- ☐ Reynolds Stress (7 eqn)
- ☐ Scale-Adaptive Simulation (SAS)
- ☐ Detached Eddy Simulation (DES)
- ☐ Large Eddy Simulation (LES)

k-epsilon Model

- ☐ Standard
- ☐ RNG
- ☒ Realizable

Near-Wall Treatment

- ☐ Standard Wall Functions
- ☐ Scalable Wall Functions
- ☐ Non-Equilibrium Wall Functions
- ☒ Enhanced Wall Treatment
- ☐ Menter-Lechner
- ☐ User-Defined Wall Functions

Enhanced Wall Treatment Options

- ☐ Pressure Gradient Effects
- ☐ Thermal Effects

Options

- ☒ Viscous Heating
- ☐ Curvature Correction
- ☒ Compressibility Effects
- ☐ Production Limiter

Model Constants

C2-Epsilon: 1.9

TKE Prandtl Number: 1

TDR Prandtl Number: 1.2

Energy Prandtl Number: 0.85

Wall Prandtl Number: 0.85

User-Defined Functions

Turbulent Viscosity: none

Prandtl Numbers

TKE Prandtl Number: none

TDR Prandtl Number: none

Energy Prandtl Number: none

Wall Prandtl Number: none

Fig 3.4.2.3 Turbulence model configurations

3.4.3. Mesh interface

During the numerical calculation, the interfaces of channel end face and ports interfaces are not always connected. In fact, if we only consider one port, the connected condition will only exist dozens of degrees during one revolution and it is periodic. The connection during interface is also accomplished with sliding. Thus, in order to automatically create the flow interfaces when they are overlapped and walls in other condition. Setting mesh interface for these surfaces are needed.

As we mentioned above, the contact regions of solid zone and fluid zone should be considered as a type of “Coupled Wall” for conjugate thermal calculating. The interface relation between 4 solid surfaces and 4 fluid surfaces should be set with “one to one” to indicate the mapping relation or the calculation would be incorrect.

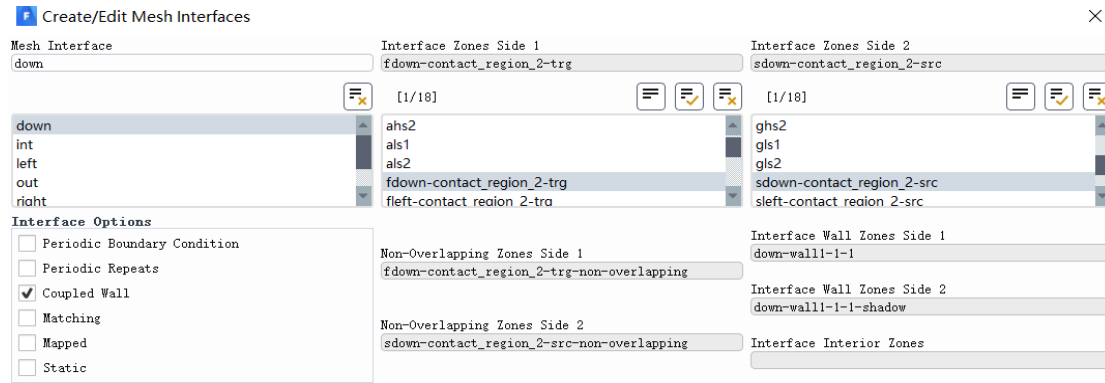


Fig 3.4.3.1 Example of mesh interface for coupled wall

Then, the interfaces of channel end face and ports interfaces should be built as “one to more” due to each surface could be set to mesh interface once. Each end face of channel will relate to four port interfaces, and there is no option should be defined for automatically recognizing the flow path only.

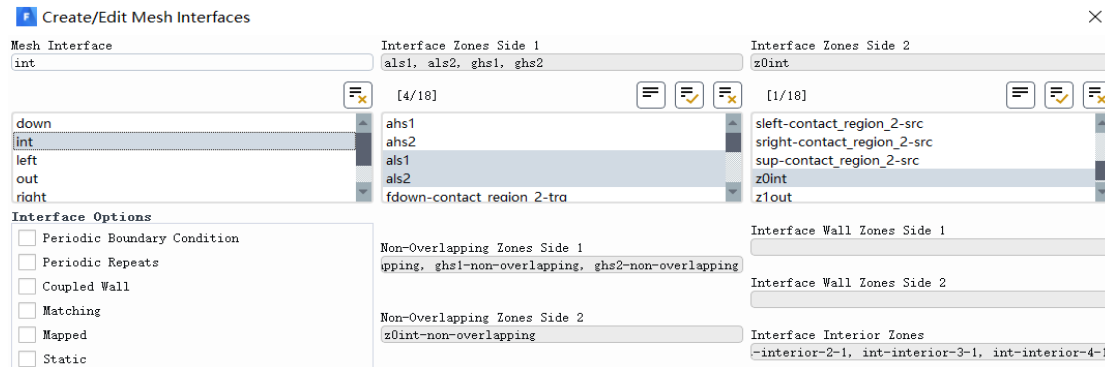


Fig 3.4.3.2 Example of mesh interface for end faces

3.4.4. Boundary conditions

Apart from the “interface” type surface, all other boundaries would be initially set as “wall”. We need change the related properties or the types of the boundaries according to the flow condition.

As it's shown in Fig 3.2.3, there are 4 ports indicating the inlets and outlets of the flow zones. The important parameters are shown in Table 3.4.4.1:

Item	Type	Total pressure (bar)	Total Temperature (K)
GH (HPG) High pressure gas inlet	Pressure inlet	9.60	1250
AL (LPA) Low pressure air inlet	Pressure inlet	3.00	440
AH (HPA) High pressure air outlet	Pressure outlet	10.20	905
GL (LPG) Low pressure gas outlet	Pressure outlet	3.69	970

The outlet pressure level would be considered as average specification. The turbulence level would be set as default. The wall of 4 ports zone would be considered as adiabatic. In general display, it should be like:

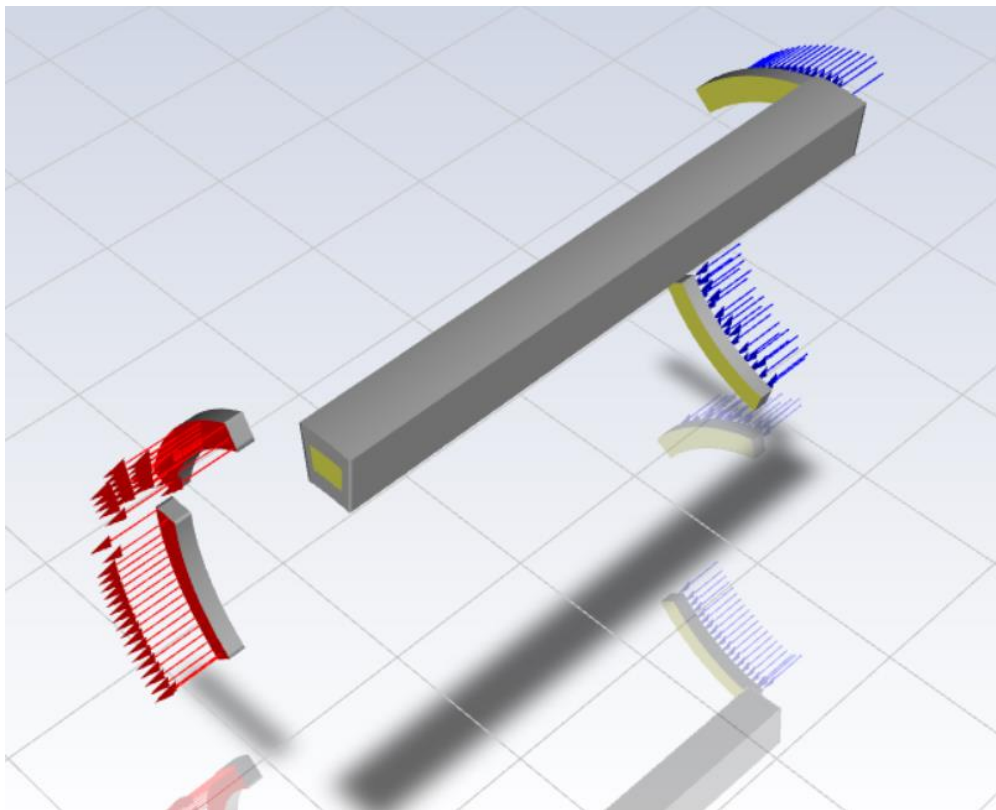


Fig 3.4.4.1 Display of model after setting boundary condition

To simplify the calculation, we consider that the thermal conduction from channel to channel (tangential direction) is smaller than the flux due to convection in radial direction. We assume that only two surface as convective heat transfer (Robin) boundary, which we consider the water as coolant and the heat transfer coefficient could be “3000 W/m²K” with an average coolant temperature as “360 K”. Other walls are assumed as adiabatic.

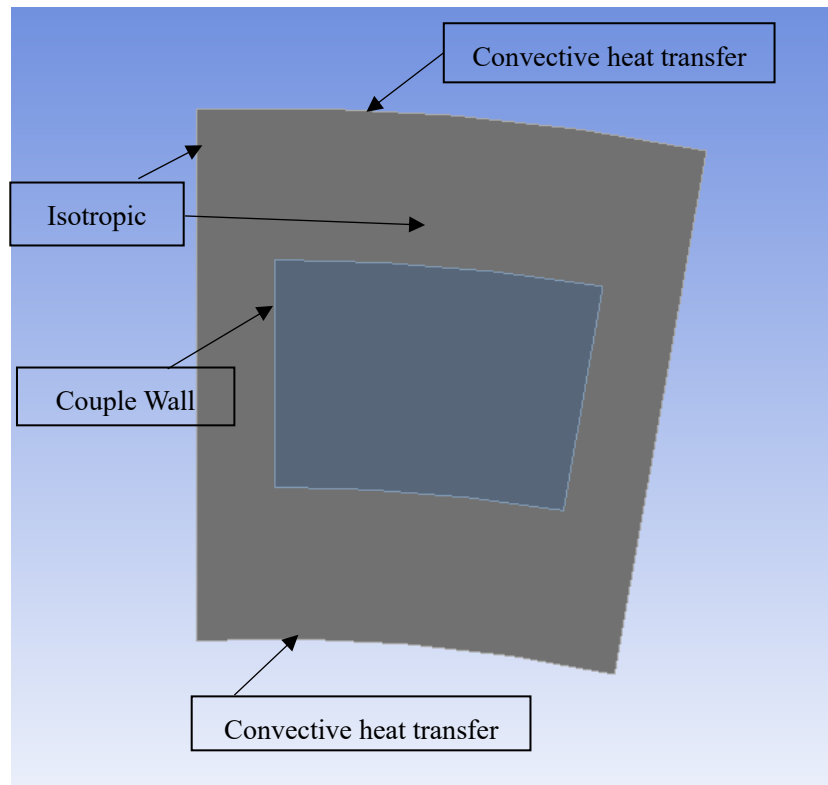


Fig 3.4.4.2 the boundary conditions for solid part

3.4.5. Post-process data configurations

In order to analysis the thermal behavior and solid temperature distribution, there are some data should be record during the calculation. All the data we chosen, and the reasons are representing as follows:

1. The contours plots animation of temperature. The temperature contours can display the temperature distribution in each recorded step which would be helpful to find the max temperature region and discussion the causes.
2. The plots of maximum, mean, minimum temperature in solid part depends on time. It's difficult to directly get a general value from the contour's plots, thus the exact data plots are required.
3. The contours plots animation of z direction velocity. Z direction velocity contours could show the flow condition of the fluid by which we could not only know the variation of z direction velocity, but also whether the back flow would occur before ports shutting.
4. The contours plots animation of pressure and pressure distribution plot animation along a line. Consider the pressure wave may be an important factor influence the thermal behaviors, it's necessary to detect the pressure level in the fluid zone to analysis the pressure wave propagation. By comparing with other data, find the law of properties change.
5. The point heat flux rate plot depends on time. As it is mentioned above, the pressure wave may result in the variation of heat flux rate in the contacted wall, we cannot exactly find a point in the contacted interface, while we can find one near the interface.

The other data, such as the “wall temperature plot animations for each side” and “total heat flux plot for each side”, are both used for thermal behavior analysis if needed.

3.4.6. Other work

Initialization is a necessary process before calculating. The more exactly we set initial parameters for each zone, the faster could system be “conservative”, while the simple initializing function could not execute a perfect work, we need to use “Patch” function to initialize the pressure and temperature for each zone manually. A good consideration for these zones is to set the parameters same as its related boundary conditions.

Time steps for calculation is another important parameter. Although we’ve set Courant number for solver, the time steps size for calculation means a frequency we detect the system. If the value is too small, it spends much time on calculation; If the value is too big, we can’t detect how pressure wave travels. In the model, 0.0000005s time step is chosen. Thus, the system will go through 3750 steps for one revolution.

It is necessary to mention that the calculation results in the primary few revolutions are not proper due to the system would have not been steady or conservative. Only if the results of two cycles are nearly the same, we can consider it have been conservative. In the model, we can take the time plots, such as “point heat flux rate plot depends on time”, as a reference to judge the consistency of cycles.

4. Simulation result and analysis

In our simulation, we could use the angle to describe the position of channel and ports. According to the Fig 3.2.2 the start position (0°) of rotor located in the beginning of the “High pressure gas inlet port” (HPG port). Before investigating the results we want, as we mentioned, it takes some time for model to reach the convergent condition. It does not mean that the system won’t have change anymore, instead, the results should become periodic. After tens of thousands of steps, the simulation of system could be convergent, however, we still need to check it before the analysis. Besides, the result might be reasonable while not consistent with real working condition due to improper boundary condition simplification, and we will discuss it according to the result.

4.1. Inviscid model

In order to better investigate the pressure wave spreading and air/gas distribution, we could introduce “inviscid” model for simulating. The inviscid model neglects all the viscous phenomenon of fluid and only it concerned on the mass and transportation and pressure spread, so the heat transfer between fluid and wall would be neglected. It’s a very simple model to get general results which could not give us the exact value, but it can show us the trends of flow behaviors. To enable the model, just choose “inviscid” in viscous model options.

4.1.1. Convergency check

First of all, we need to prove that the simulation system has been convergent or periodic. A good method to prove it is to investigate some data over serval revolutions, if the value of data is periodic occur, the system could be considered as steady or convergent.

In order to do the work, we could investigate the pressure value of one point inside channel. As it shown below in Fig 4.1.1.1, the point P is located in the middle line of channel (the middle line parallel to the rotation axis and the distance between them is 23.5 mm), 0.03 m away from the channel charging side.

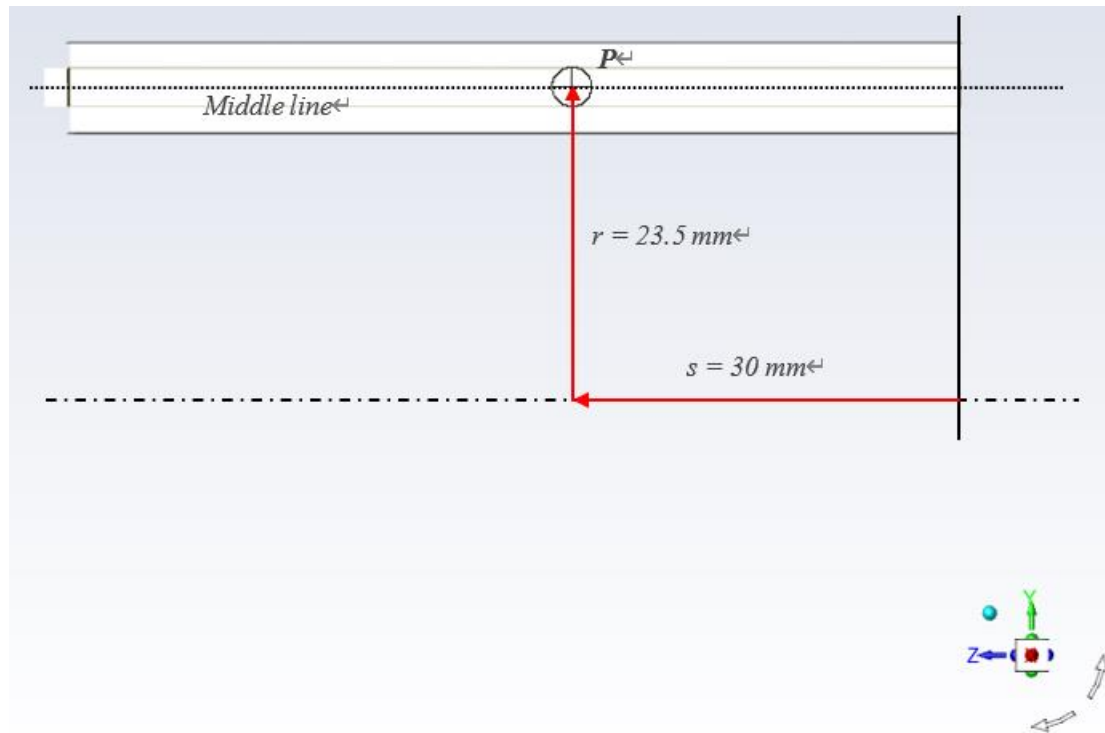


Fig 4.1.1.1 Scheme of P point location

After introducing the location of P point, we could discuss the results of P point as shown in Fig 4.1.1.2. Let us consider the beginning of data is the 0° of one cycle and the end of data is 720° , where 0° represents the beginning of HPG port in previous cycle and 360° represents the beginning of HPG port in next cycle.

We can realize that the pressure plots of P point could be considered as periodic, which two similar cycle are shown in the Fig 4.1.1.2. Two cycles plots have similar trends, similar maximum value and similar minimum value at same position according to angle. Thus, we could say the simulation system have been convergent and we could investigate its results.

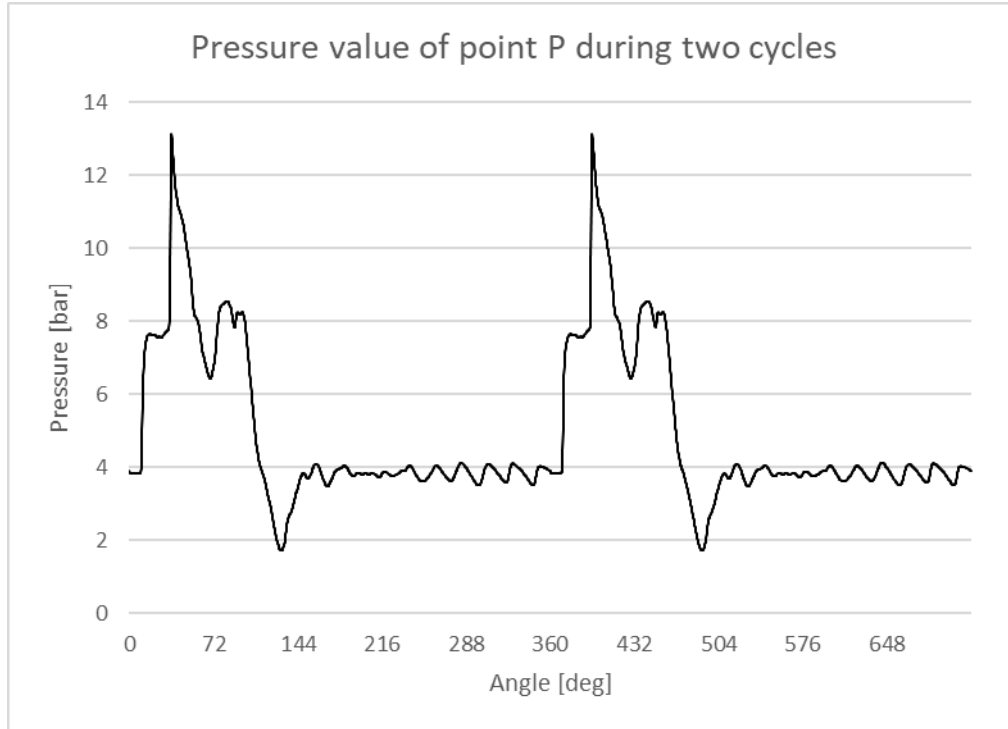


Fig 4.1.1.2 Pressure value of point P variation plot in inviscid model during two cycles

4.1.2. Pressure results inside channel

One of the most important features to discuss the flow behaviors inside channel is pressure wave spreading. As a matter of fact, the wave rotor is a pressure exchanger, utilizing pressure wave to transport the energy.

The contours plots of pressure could show us the pressure distribution in a cross section. Let us introduce the tangential plane which contains the middle line in Fig 4.1.1.1 as contours section. If we combine a series results of contours in different angle, we could create an animation for pressure wave spreading, while a better way to discuss the behavior is to create a map plot. We can consider that the results of one channel could be regarded as other channel with a time shift. There are 30 channels in wave rotor with angular interval 12° , thus, we can consider the results in 0° as first channel; 12° as second channel at same time and so on. Then we would get the results of 30 channels at same certain time and create a contours map as shown in Fig 4.1.2.1.

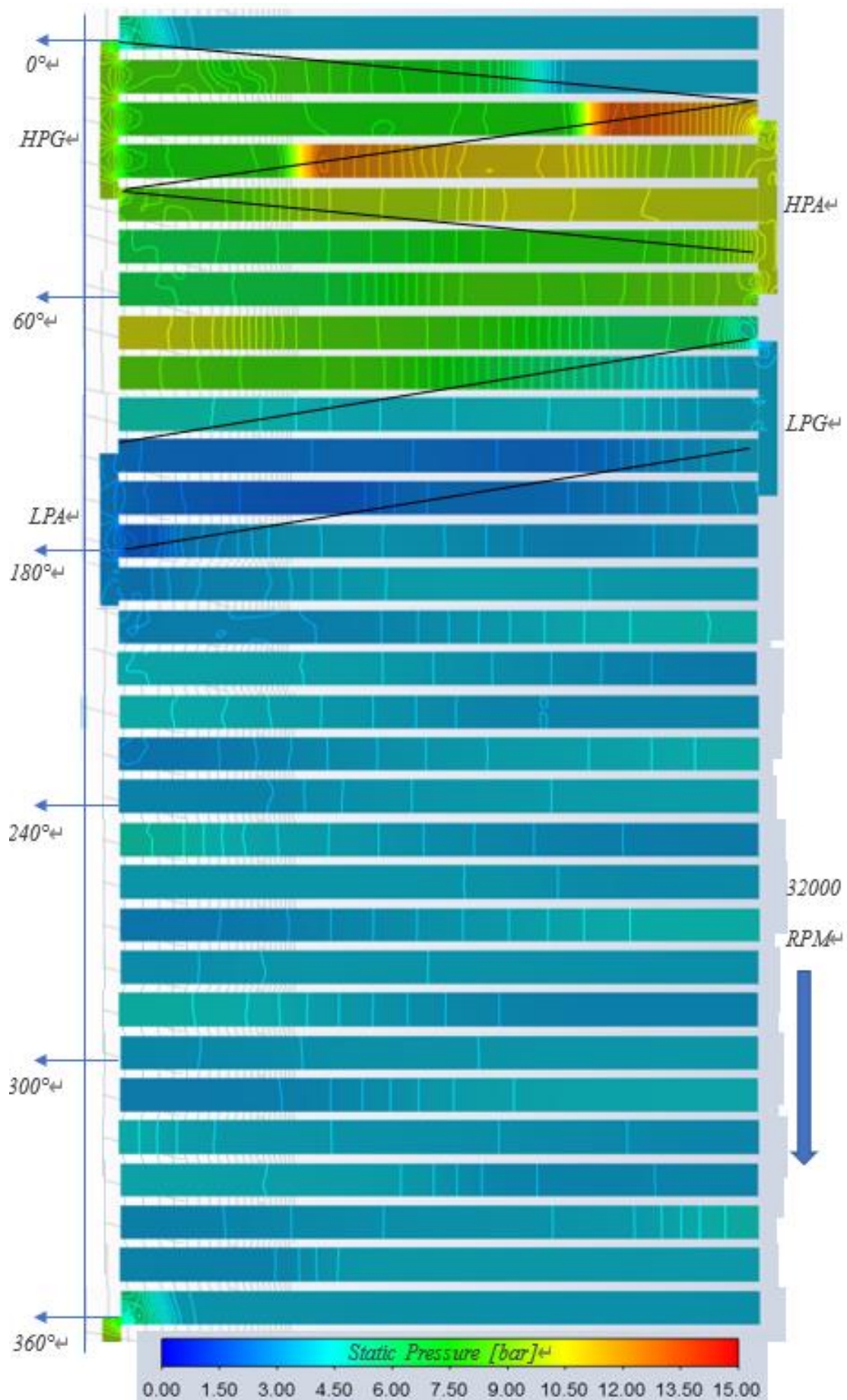


Fig 4.1.2.1 Pressure contours map with all channels in inviscid model

In the Fig, the empty regions between channels are wave rotor walls. We could clearly see the shock wave spreading at beginning and we can use some black lines to divide the map plot according to the pressure level. In fact, the black lines could also be considered as the shock lines indicating the pressure wave spreading.

The max pressure value occurred after a short time when primary pressure wave reached the discharging side wall which the fluid near the discharging side region would be continuously compressed and then discharging to LPA port before expanding backside. Meanwhile, the reflected pressure wave spread back and reach the charging side wall after HPG port shutting. And the pressure wave would reflect again and further promoting the discharging process.

When LPG port opened, the fluid inside channel would expand rapidly, the pressure level would also decrease rapidly even lower than 300000 Pa due to fluid inertia. Meanwhile the LPA port would open and charge the channel with the extreme low-pressure level inside channel, further pushing the gas out by its inertia, it is so-called scavenging process. After LPA port shutting, the fluid oscillated inside channel and preparing for next cycle.

Comparing with the reference article, our results generally show the consistency with the reference results while there is a small shift in shock line or, generally speaking, pressure spread faster than reference. It could be an effect due to the inviscid model,

In other view, we could also use pressure distribution plots along a line inside channel to investigate more details about primary shock spreading before it reflected twice during $0^\circ \sim 40^\circ$. Recalling the Fig 4.1.1.1, we could investigate the pressure level in middle line.

As shown in Fig 4.1.2.2, the “Y” axis represents the pressure value with unit “bar”, the “0 m” represents the charging side position and the discharging side position is “0.069 m”. The primary shock reached discharging side at around 20° and the fluid could not compress the wall, instead, fluid compressed by wall and reflected with higher pressure level, traveled back towards the charging side.

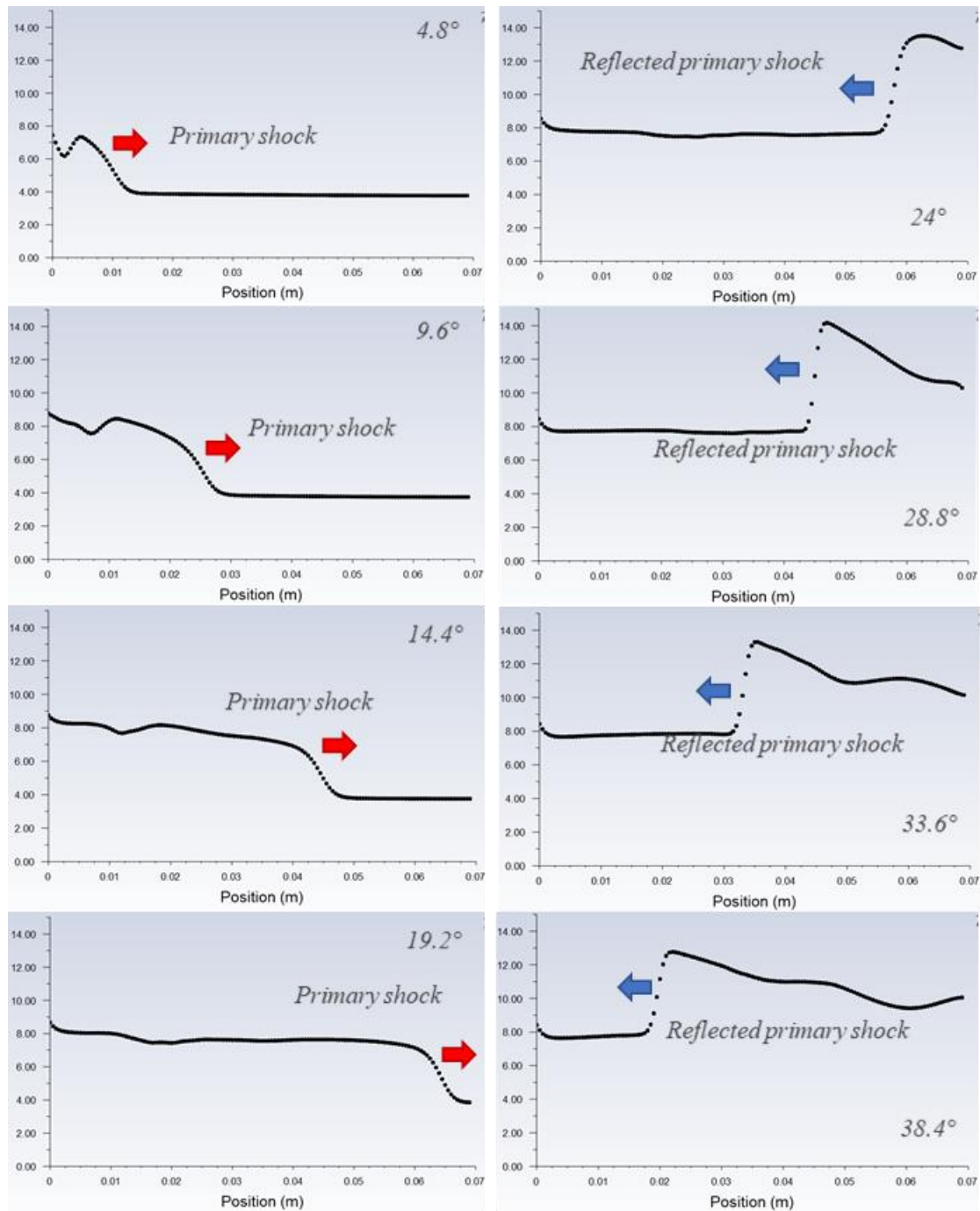


Fig 4.1.2.2 Scheme of pressure wave spreading during $0^\circ \sim 40^\circ$ based on pressure level in “middle line” in inviscid model

4.1.3. Temperature and velocity contours

Let us introduce the same section as pressure contour plots, we could also generate the temperature contours map and velocity contours map in same way.

Fig 4.1.3.1 show the temperature contours map of wave rotor. In inviscid model, the fluid temperature could be affected only by three main points:

1. Compression and expansion behavior, which the variation follows idea gas equation of state.
2. Convection and conduction heat transfer behavior between low temperature air and high temperature gas in interface.
3. Mixing behavior between low temperature air and high temperature gas in interface.

Inside which, the compression and expansion behavior dominate the variation, the heat transfer behavior and mixing behavior have related small effect due to small reaction period in cycle. Besides, there is a big difference of temperature value between fresh air (440 K) and burnt gas (1250 K). In other words, we could consider that the low temperature region represents the fresh air and high temperature region indicates the burnt gas. Thus, the temperature contours map could show us the fresh air distribution in wave rotor channels.

The black lines show the general interfaces between air and gas, which it generally shows the consistency with reference article while a part of air exhausted to LPG port.

Fig 4.1.3.2 shows the Z velocity contours map, which z direction velocity could show the flow direction of fluid inside channels. There is no doubt that in the region around HPA shutting, we discovered there was a back flow and that is the reason why a part of air exhausted to LPG port. Besides, small back flow also presented when LPG shutting. Recalling the Fig 4.1.2.1, that might result from the “shift” of shock.

Generally speaking, the inviscid model could be calculated faster than viscous model and easy to show the general trends of wave rotor. However, the results are not precise, and we still need to investigate the viscous model.

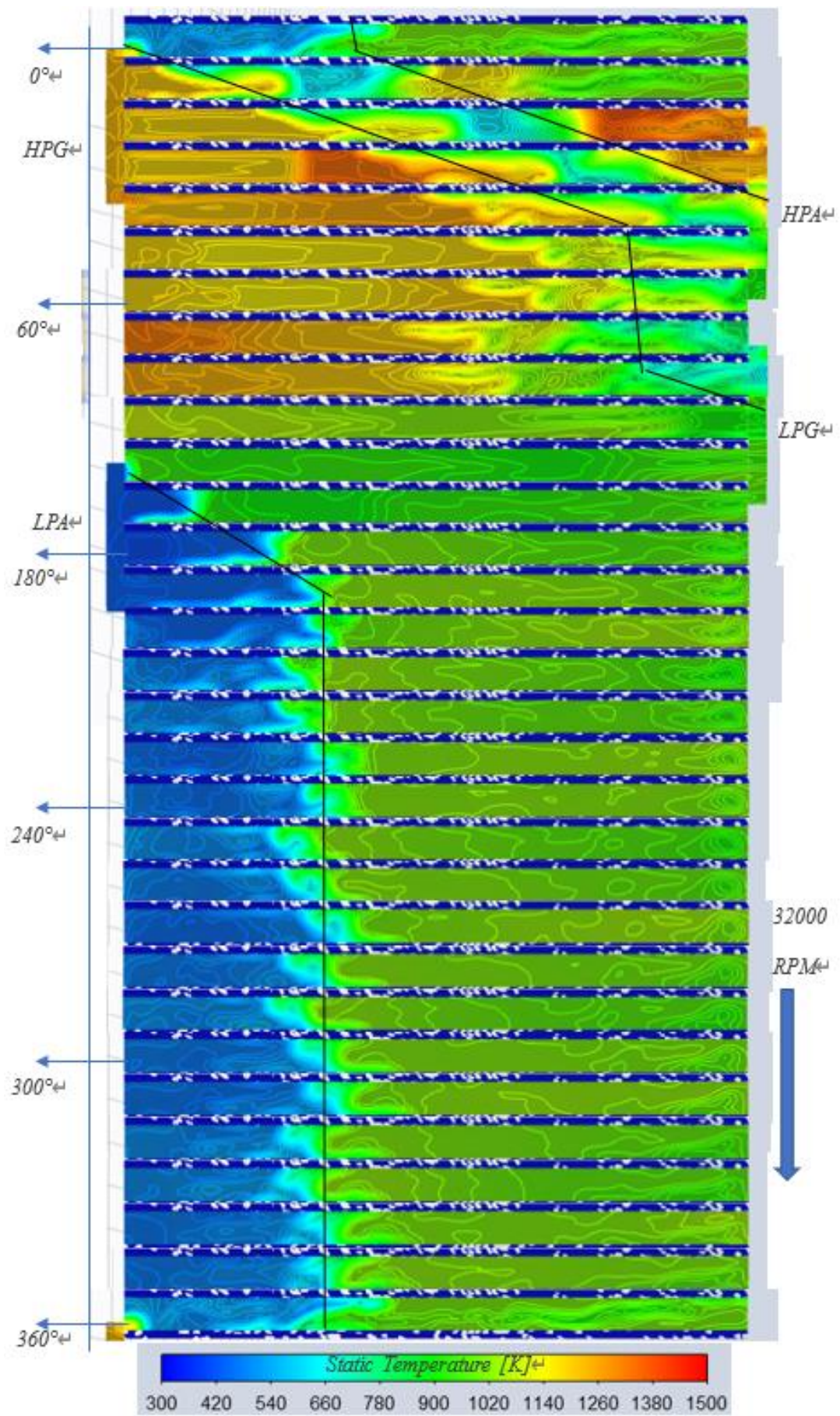


Fig 4.1.3.1 Temperature contours map with all channels in inviscid model

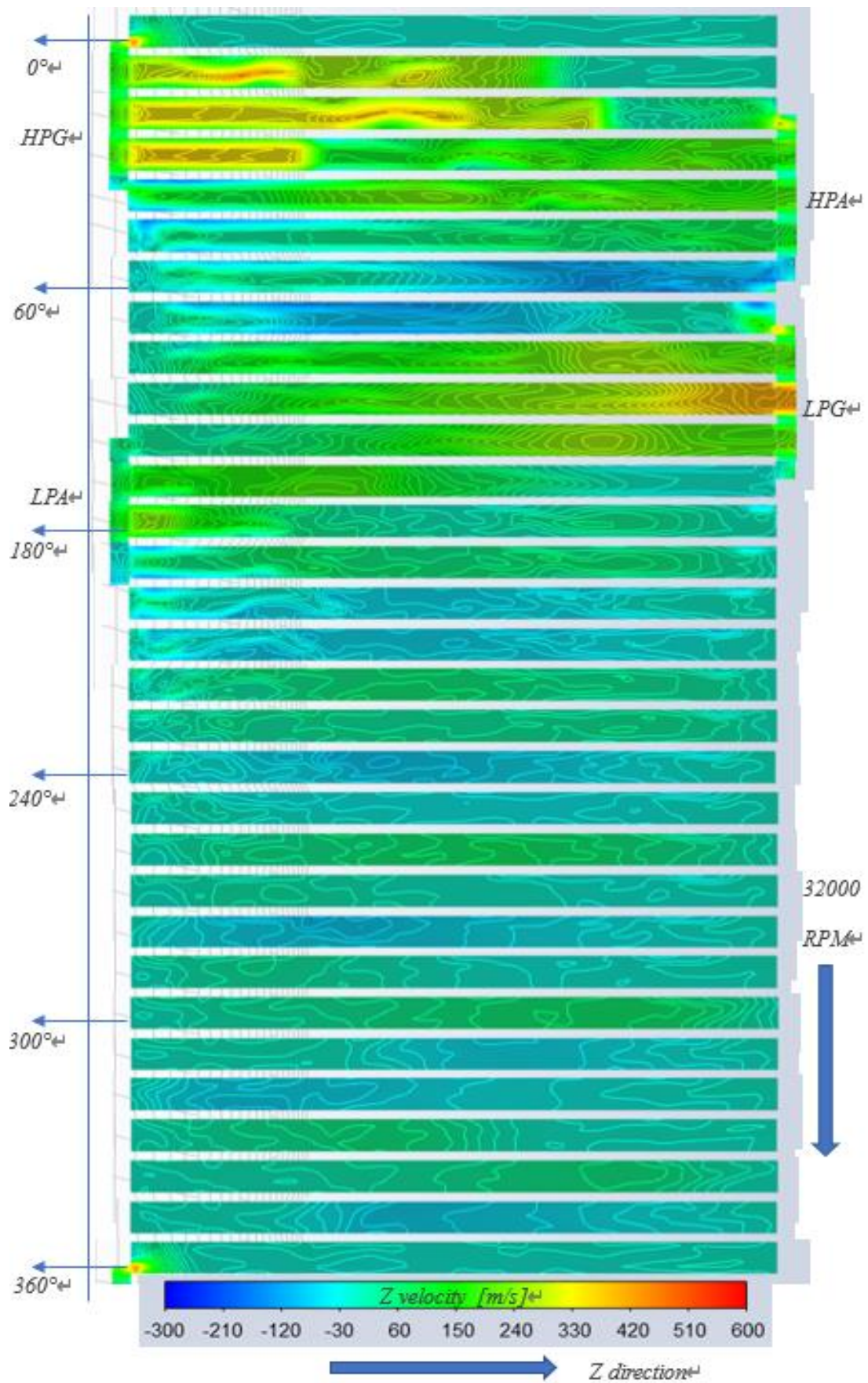


Fig 4.1.3.2 Z velocity contours map with all channels in inviscid model

4.2. Viscous model

As it was mentioned above, the viscous model using $k-\varepsilon$ model to simulate the viscous behaviors of fluid. The viscous model considers also the viscosity of fluid and wall-functions; thus, we could not only get a more precise results about flow behaviors than inviscid model but also investigate the heat transfer behaviors related to solid part and thermal state of solid part.

It is worth to mention that all the geometries and boundary conditions are the same in two models, the only difference between two models is viscous consideration.

4.2.1. Convergency check

In the viscous model, the system takes more time to reach the convergent condition. Recalling the P point in Fig 4.1.1.1, we could also plot the pressure value variation of P point during two cycles in Fig 4.2.1.1 of viscous model to check the convergency.

It is obviously that the plots of two cycles are similar, thus, the system have already reached the convergent condition. Comparing with Fig 4.1.1.2, there are less “edges” occurred in the viscous model plots. We can consider that the fluid with viscosity could work as a damper, dissipating the kinetic energy to thermal energy, making the pressure plots more smooth than inviscid model.

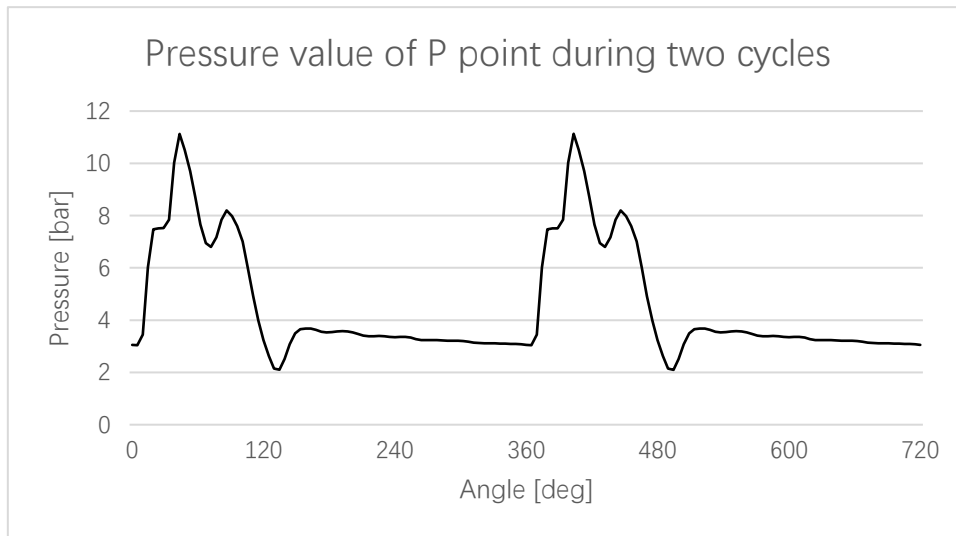


Fig 4.2.1.1 Pressure value of point P variation plot during two cycles in viscous model

4.2.2. Pressure results inside channel

In viscous model, we could use the same section plane as inviscid model for better comparing and discussing the fluid behaviors inside channels. Fig 4.2.2.1 shows the pressure contours map by combining 30 channel contours together.

The pressure contours map of viscous model shows similar trend of pressure level change. We could use black lines to indicate the shock lines either and it shows some slight differences between two models. According to the black lines view, as we said above, with the viscous effect, the fluid working as a damper, which decreased the intensity and speed of pressure wave so that the pressure level of the front of wave would decrease faster.

Besides, the general pressure level of fluid over the revolution of viscous model is lower than the inviscid model, the pressure oscillation after LPA ports shutting became less obvious than inviscid model, which this phenomenon also shows the consistency with the P point pressure plot.

The other features of viscous model map are similar with inviscid model and we would no longer explain them again. Also, for more details about the pressure wave spread, we also generate the pressure level plots in the middle line mentioned above during $0^\circ \sim 40^\circ$ in Fig 4.2.2.2.

The results show the features that:

1. The first reflected pressure level of viscous model (maximum 14.8 bar after reflecting) is higher than inviscid model. (maximum 13.8 bar after reflecting)
2. The pressure wave intensity of viscous model decreased faster than inviscid model. (from $24^\circ \sim 38.4^\circ$, pressure level of wave front decreased from 14.8 bar to 12.8 bar in viscous model while from 13.8 bar to 13 bar in inviscid model)
3. The pressure wave spreading speed of viscous model lower than inviscid model. (the shock travelled less distance at same angle)

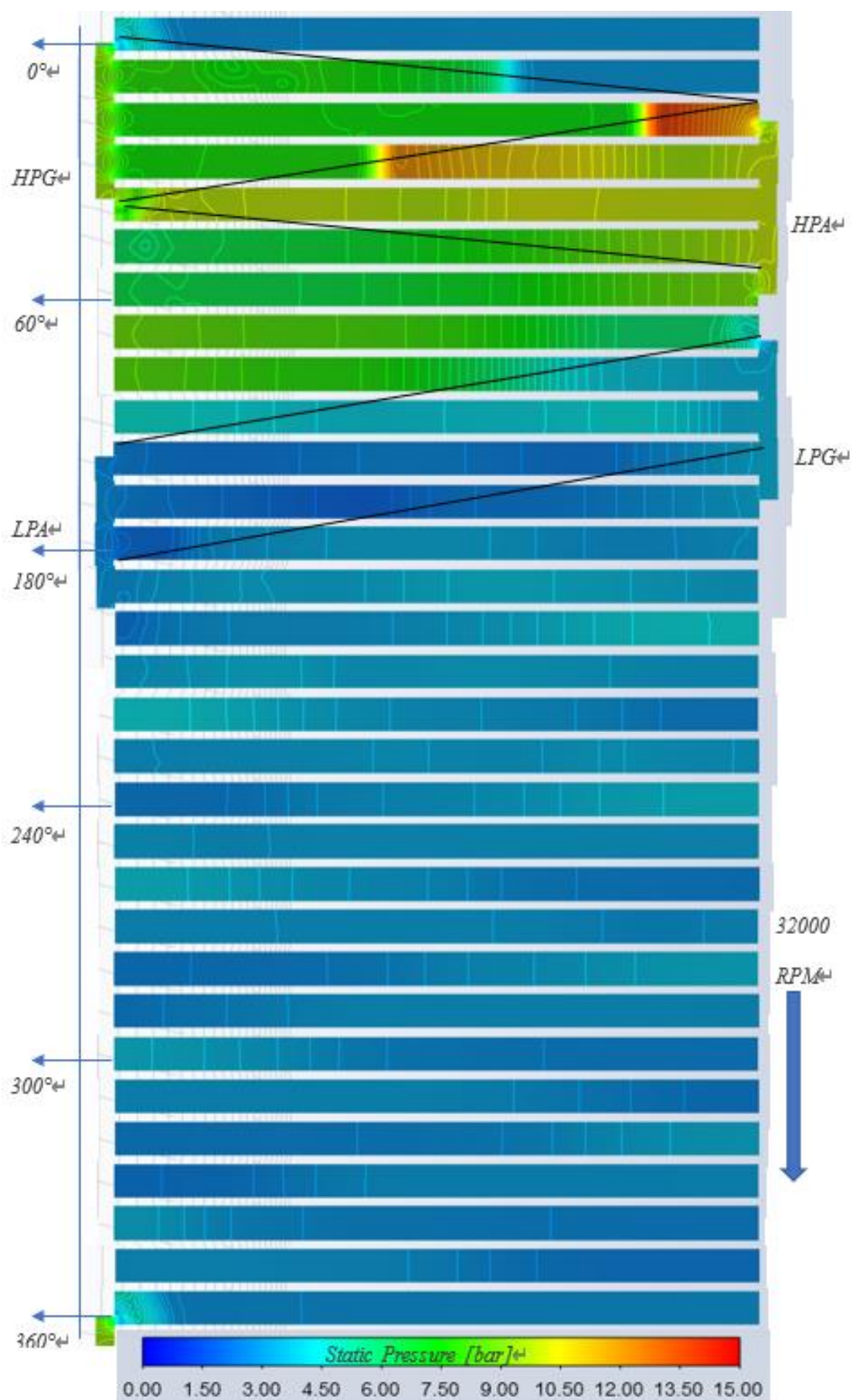


Fig 4.2.2.1 Pressure contours map with all channels in viscous model

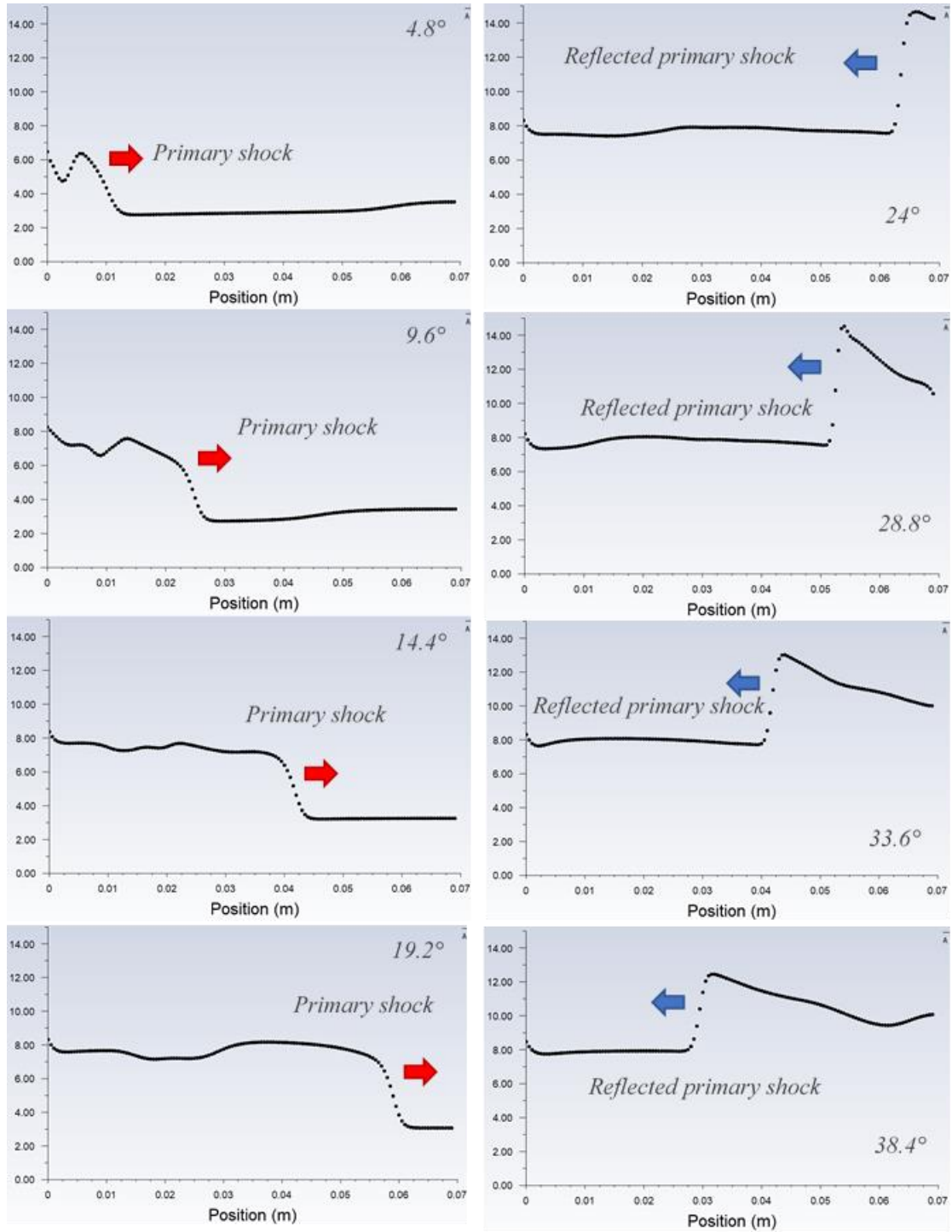


Fig 4.2.2.2 Scheme of pressure wave spreading during $0^\circ \sim 40^\circ$ based on pressure level in "middle line" in viscous model

4.2.3. Temperature and velocity contours

Even the viscous model was used, the mixing and heat transfer behaviors between gas and air could be still considered having small effect to fluid temperature variation comparing with compression and expansion process.

Fig 4.2.3.1 show the temperature contours map with all channels of wave rotor. We could also see the pressure wave before it reflected twice, also the temperature interfaces are clear. By using black lines, we can generally show these interfaces of gas and air.

Comparing with inviscid model, the results of viscous are more precise. According to the map, most of the fresh air have been delivered to HPA port, although part of residual gas was also delivered, it makes sure the delivery process go well and no fresh air would be wasted.

Fig 4.2.3.2 show the Z direction velocity contours map with all channels of wave rotor. Comparing with inviscid results, there is almost no back flow behavior in all connected region between channels and ports. Besides, when fluid velocity was not very small, the boundary layers near the wall could be discovered clearly.

In the beginning of the cycle (around 0°) the HPG port opened and the Mach number of injected gas could be larger than one. While after a few angles, the fluid speed decreased, and Mach number would lower than one. Recalling the Fig 4.2.2.1, the pressure contours map, and Fig 4.2.3.1, the temperature contours map, we could see that, in the second channel, the pressure wave traveled further than new gas. That is because when flow Mach number lower than one, the pressure wave would still travel as local sound speed while the fluid could not reach.

Moreover, if we add the shock lines in velocity map, we could discover that the shock lines are also the interfaces of high speed fluid and low speed fluid.

Generally speaking, the viscous model results are more reasonable and closer to the real working process.

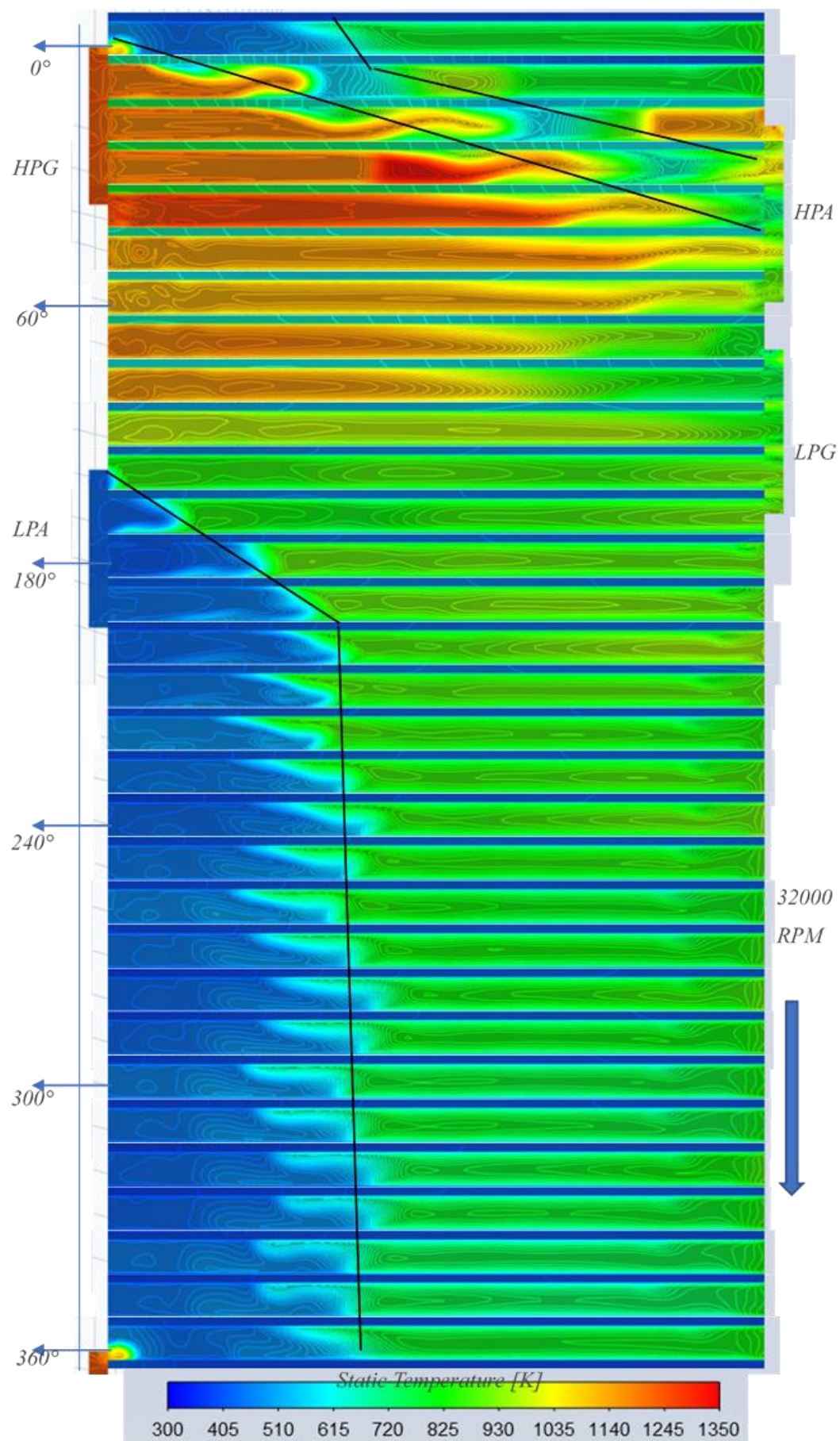


Fig 4.2.3.1 Temperature contours map with all channels in viscous model

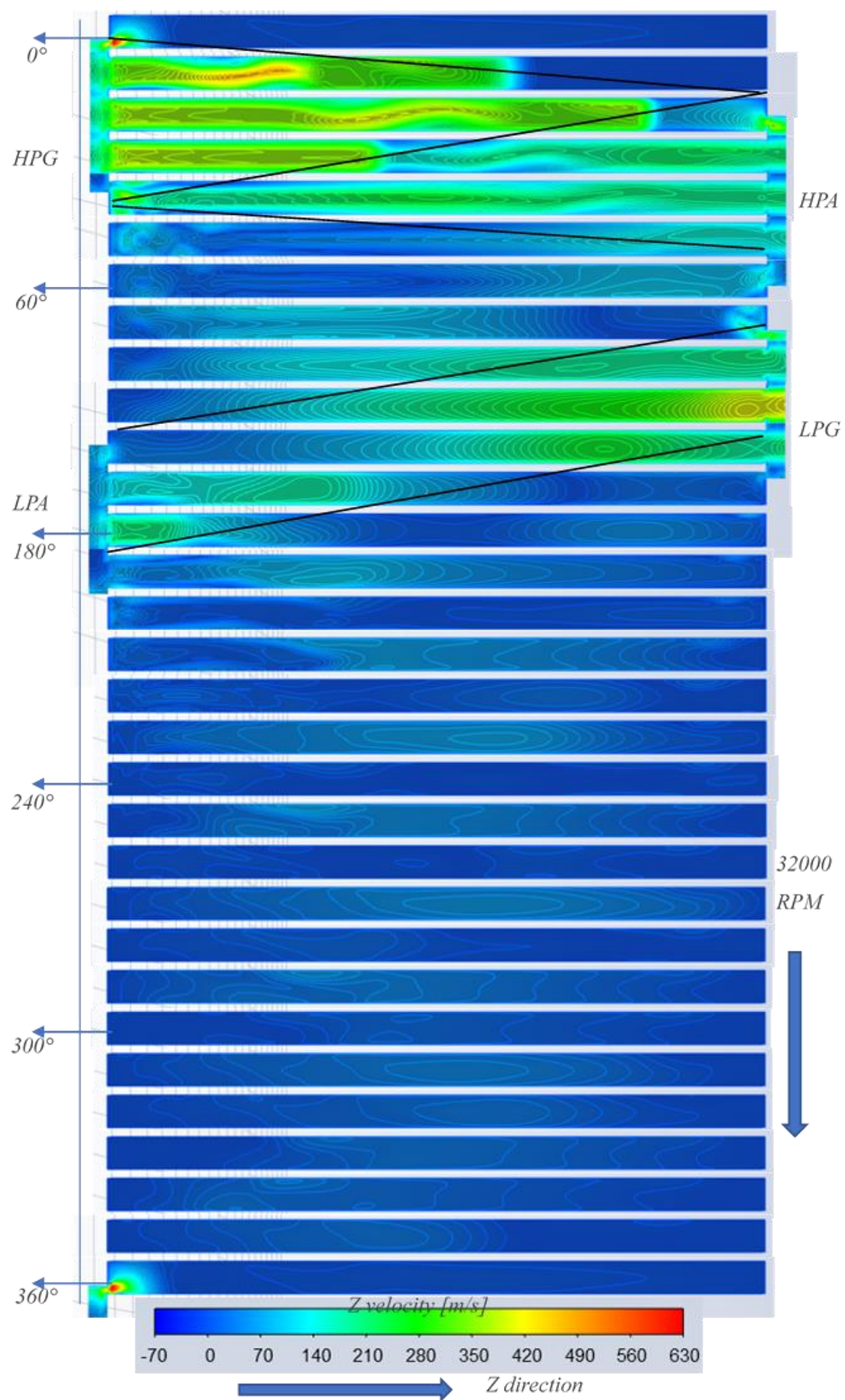


Fig 4.2.3.2 Z direction velocity contours map with all channels in viscous model

4.2.4. Conjugate heat transfer results

We have already proved the correctness of the model in previous part. Although there should be still some imperfections making differences to the accuracy of the results, we could generate roughly correct trends and values from the simulation. In this part, we will talk about the conjugate heat transfer results of the wave rotor model, analysis the relationship between these behaviors.

4.2.4.1. Temperature variation of wave rotor

First of all, let us talk about the temperature variation of wave rotor. Fig 4.2.4.1.1 shows the maximum temperature, mean temperature, minimum temperature variations of single channel over one revolution.

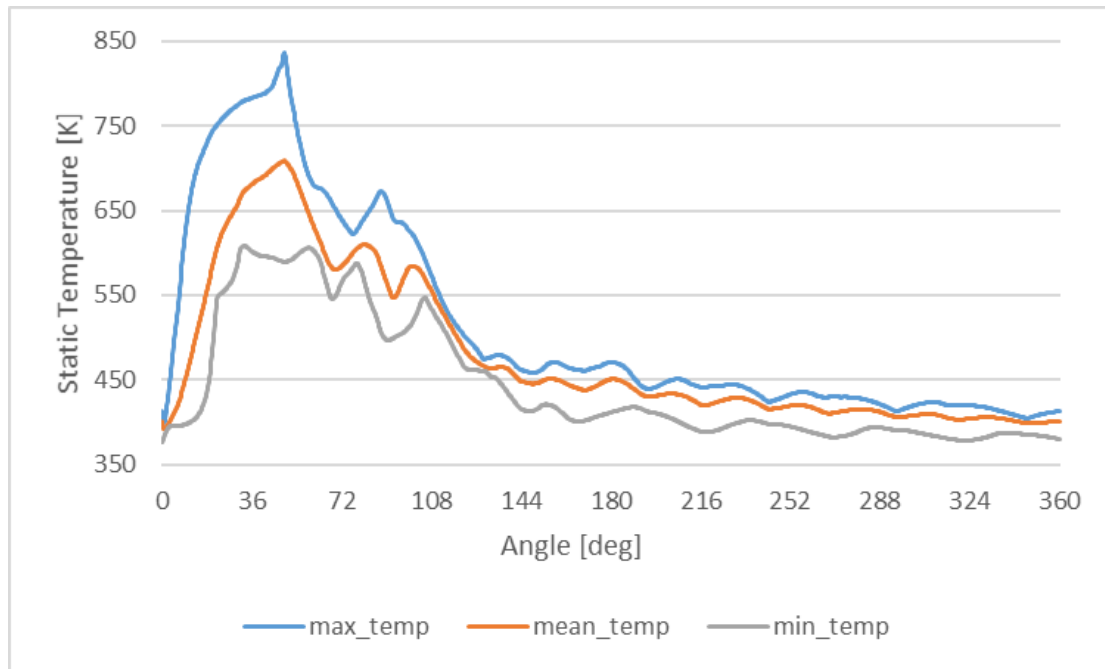


Fig 4.2.4.1.1 Maximum temperature, mean temperature, minimum temperature variations of single channel over one revolution

The relation between angle and position is the same as it is mentioned above. According to the original data, maximum temperature (maximum of max temperature) of wave rotor was around 835 K occurred in 49° angle and minimum temperature (minimum of min temperature) was around 378.5 K occurred in 321° angle.

The max temperature of wave rotor increased rapidly during $0^{\circ} \sim 15^{\circ}$ while the min temperature had a slight increase at same period. Also, the max temperature have a rapid decrease in 49° when it reached the maximum value and there was no similar trend discovered in min temperature. From around $0^{\circ} \sim 100^{\circ}$, the difference between max temperature and min temperature was large while after 100° , the difference became much smaller.

Besides, the maximum temperature must appear in the coupled walls since the surface of rotor would perform convective heat transfer and the temperature in solid part would continuously decrease from inner to outer. If we want to find the region where maximum temperature occurred, we could generate the temperature contours plots of four coupled walls as shown in Fig 4.2.4.1.2.

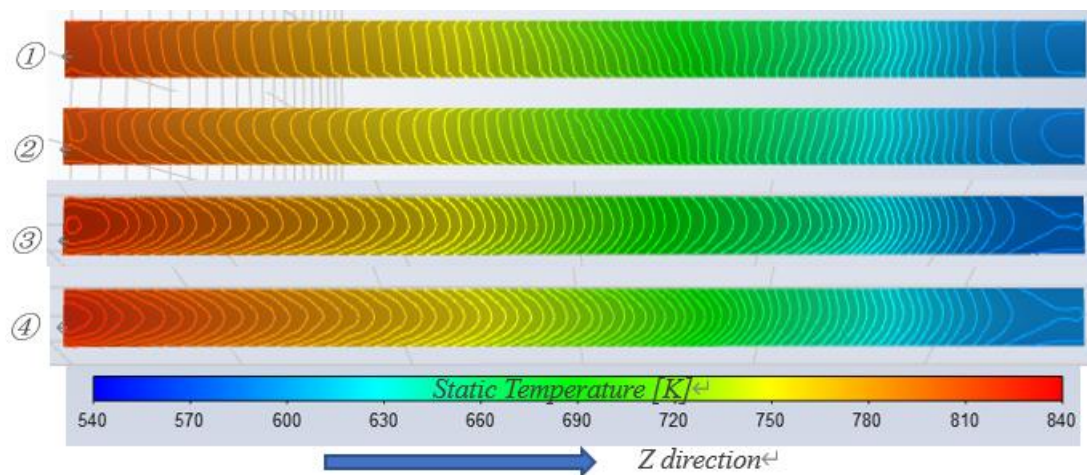


Fig 4.2.4.1.2 Temperature contours of four coupled walls

The indicator ‘①’, ‘②’, ‘③’, ‘④’ represent different coupled wall shown below:

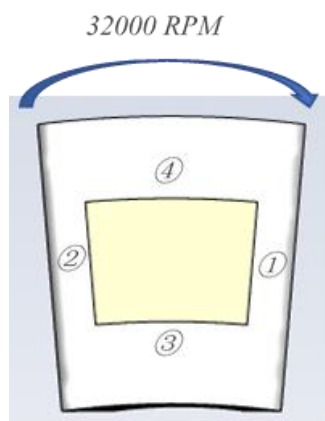


Fig 4.2.4.1.3 Scheme of four coupled walls

According to the contours, the higher temperature appeared in the region near the HPG port. Besides, the temperature of front and back walls is higher than inner and outer walls since we assume that heat transfer mainly happens in radial direction.

4.2.4.2. Heat flux variation inside channel

According to the heat flux variation trends, we could better explain the temperature variation. It is too complex to show the heat flux contours for all coupled walls over one revolution, thus, we could investigate the heat flux of one point Q on coupled wall instead. Fig 4.2.4.2.1 shows the position of the point Q which located at the outer coupled wall in the middle plane (yz plane).

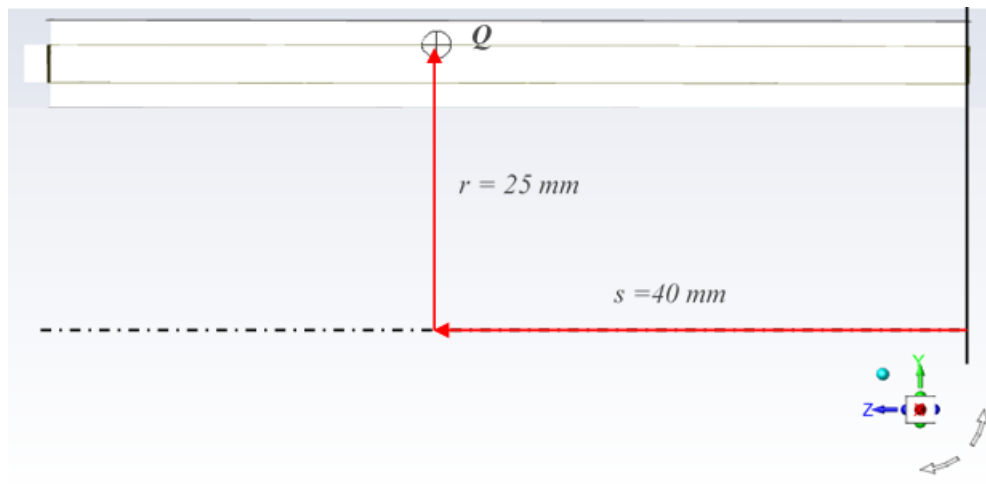


Fig 4.2.4.2.1 Scheme of Q point location

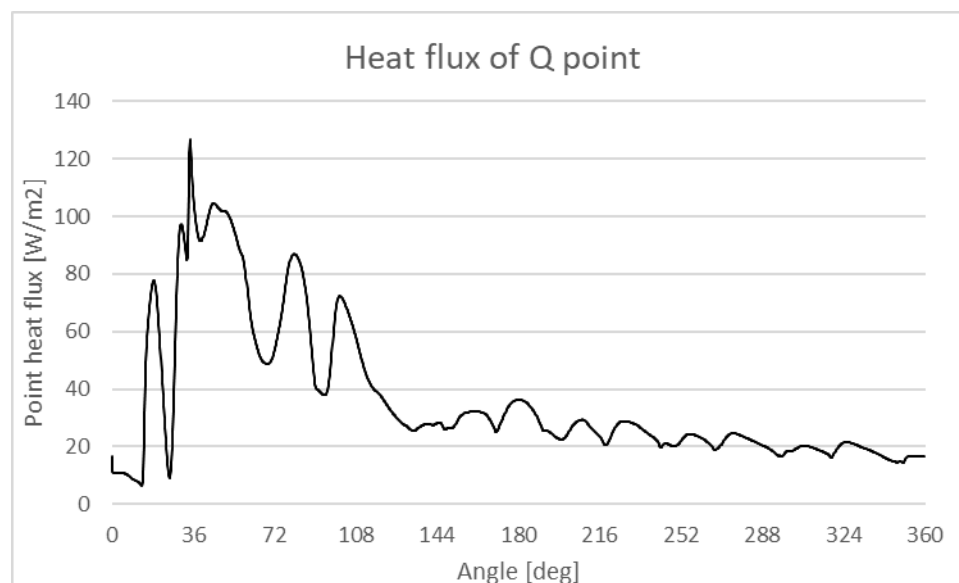


Fig 4.2.4.2.2 Heat flux variation of Q point over one revolution

Fig 4.2.4.2.2 shows the heat flux variation of Q point over one revolution. The maximum heat flux of Q point appeared at 34.5° , earlier than maximum temperature appeared at 49° . We could consider that the heat flux is directly related to the temperature change rate and even the heat flux decrease, the temperature would still increase as long as the input flux larger than output flux. The trend could be seen by combining the max temperature plot and heat flux of Q plot in Fig 4.2.4.2.3. Although Q point located at different position as max temperature region, we could shift the heat flux plot advanced for analyzing.

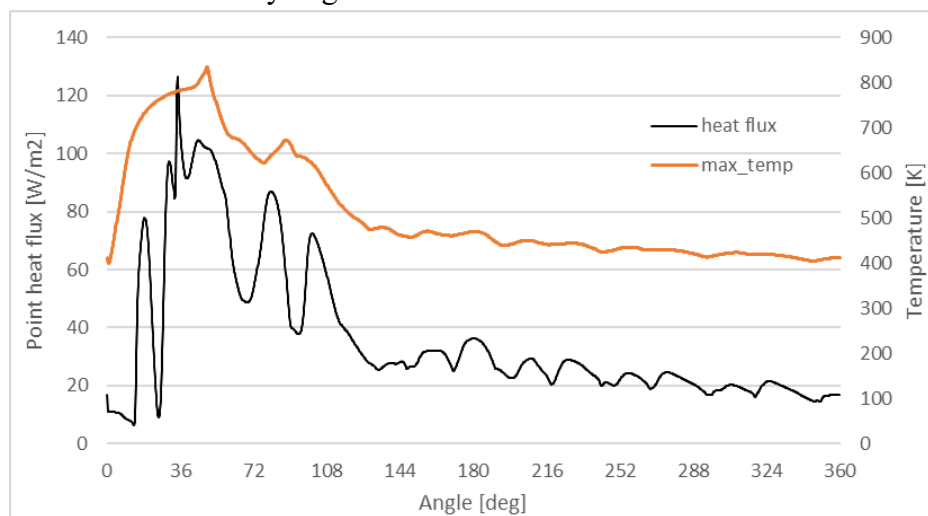


Fig 4.2.4.2.3 Combination of max temperature and heat flux of point Q over one revolution

Besides, there was a drop of heat flux value before it suddenly increasing to maximum value. The point heat flux depends on two features: “the temperature difference between fluid and wall” and “heat transfer coefficient of wall”, and the later feature is directly related to Re number.

Fig 4.2.4.2.4 shows the Temperature map with black lines show the temperature interfaces and white lines show the shock spread. Recalling the conclusion mentioned before, the shock lines also show the speed interfaces. Let’s explain the beginning of plot. According to the map, from 0° , the pressure wave first went through the Q, the Re number of Q region increased rapidly lead to heat flux of Q increased rapidly. Then, Q point got into the low temperature air region, thus, the heat flux of Q dropped suddenly. Next, Q point got into the hot gas region and heat flux of Q increased again. And the later condition could also be explained according to it.

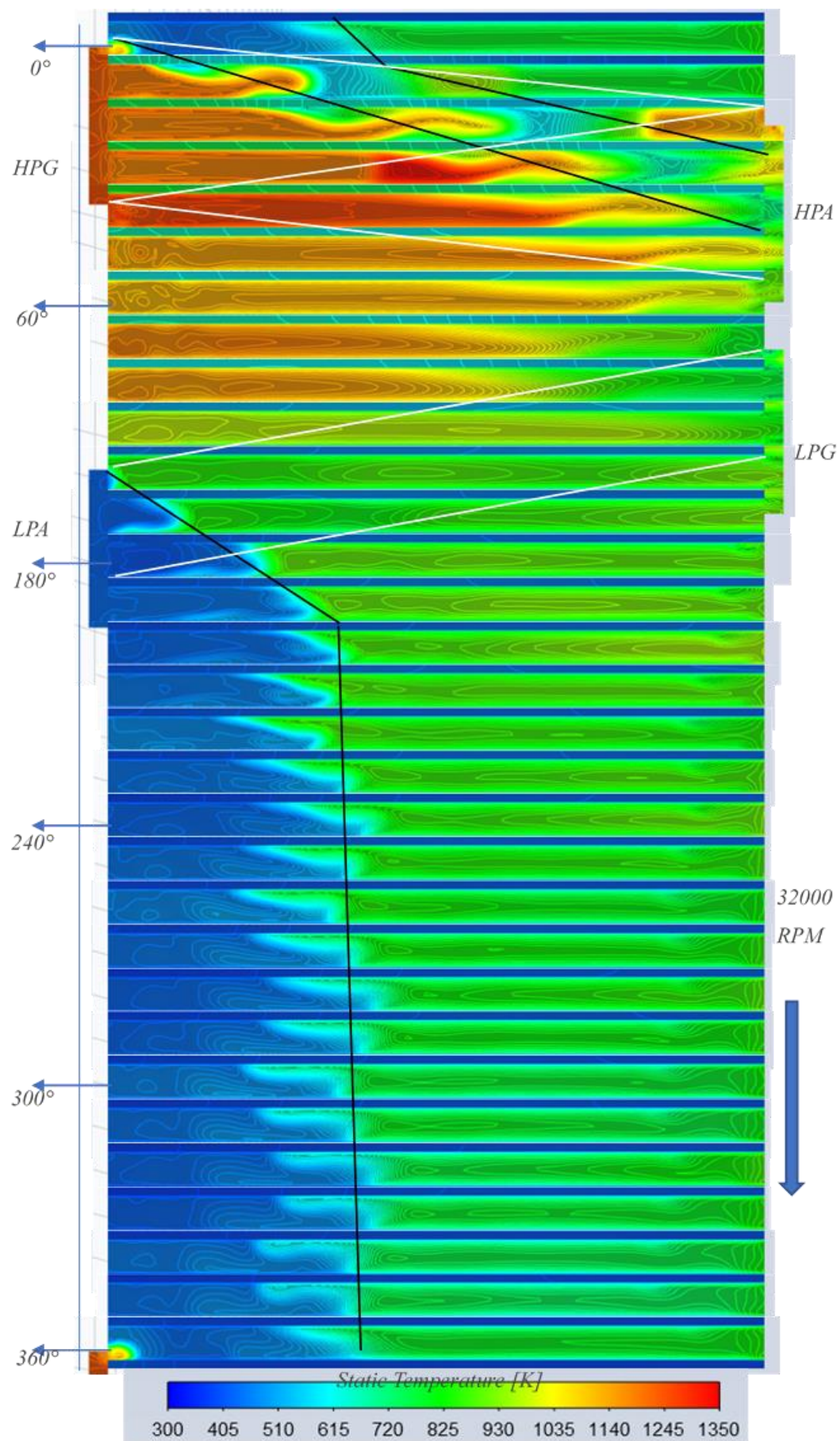


Fig 4.2.4.2.4 Temperature contours map with shock lines

5. Conclusion and further work

We have already discussed all the details during the cycle and all the thermal and flow behaviors have been explained according to the theoretical analysis, and the results all show the consistency with the reference and theoretical principles.

During the research, the inviscid model and viscous model are both used for better displaying the transient results over one revolution. The back flow phenomenon was only discovered in inviscid model while in viscous model it disappeared, and the results were more precise and whole system worked well.

In each cycle, the high-pressure residual gas could successfully exchange the energy to fresh air, which the pressure of gas decreased from 960000 Pa to 369000 Pa with expansion ratio 2.6 and increased the pressure of fresh air from 300000 Pa to 1020000 Pa with compression ratio about 3.4 and it could greatly improve the efficiency of combustor. While, on the other hand, the higher air temperature should also be considered in combustor to prevent the overheating in combustion.

We could also discover the maximum temperature around 835 K appeared in the region near the HPG port with material Aluminum, indicating that the better materials or cooling measures should be considered carefully to prevent yielding. Besides, the minimum temperature of wave rotor also reached around 378.5 K during the cycle. It is worth to mention that the large difference between maximum temperature and minimum temperature in cycles would lead to large cyclic alternating stress, accelerating structural fatigue. So, it should be also considered in design period.

Apart from the work we have done until now, in the future, there are still many imperfect parts could be considered in the model and there are still many further works could be done based on the results:

1. The model only simulated one channel results under the assumption that the main heat transfer behavior happens in radial direction, while the heat transfer in tangential direction could also be important and the maximum temperature

of solid part could be lower than our result. A completed model would be more precise and it's helpful to design a cooling system for wave rotor.

2. There is no experimental result support the analysis. We generally consider the experimental data from other articles to discuss the wave rotor behavior while we did not build a real wave rotor system to obtain the raw data. What we have done was only the numerical analysis. In the future, an experimental bench could be established for researching and development.
3. The geometries and boundary conditions could be varied for discussing their influence on performance of wave rotor. Besides, the transient condition during the real usage of wave rotor could also be researched, which could be helpful to develop some control strategies for wave rotor.
4. There are still many different types of wave rotor, such as there could be a nozzle formed by bending channel which might be helpful to deliver the fluid. Others like wave rotor combustor and wave rotor refrigeration system could also be studied for extending the usage of wave rotor.

Wave rotor is still in developing and it have not been widely promoted. The researchers are going to test the feasibility of wave rotor utilized in all fields and try to find a common method to design a wave rotor. Maybe, in the not far future, the wave rotor could become a dazzling role in each machine bring great improvements for mechanical industry.

Reference

- [1] Akbari, P., Müller, N., 2003, "Preliminary Design Procedure for Gas Turbine Topping Reverse-Flow Wave Rotors", *Proceedings of the International Gas Turbine Congress 2003 Tokyo*, IGTC2003Tokyo FR-301.
- [2] Weber, H. E., 1986, "Shock-Expansion Wave Engines: New Directions for Power Production," *ASME Paper 86-GT-62*.
- [3] Weber, H. E., 1995, *Shock Wave Engine Design*, John Wiley and Sons, New York.
- [4] Darrieus, G., 1950, "Pressure Exchange Apparatus," U.S. Patent 2526618.
- [5] Kentfield, J. A. C., 1993, *Nonsteady, One-Dimensional, Internal, Compressible*
- [6] Gyarmathy, G., 1983, "How Does the Compres Pressure-Wave Supercharger Work?," *SAE Paper 830234*.
- [7] Zehnder, G., Mayer, A., and Mathews, L., 1989, "The Free Running Compres[®]," *SAE Paper 890452*.
- [8] Hiereth, H., 1989, "Car Tests With a Free-Running Pressure-Wave Charger
- [9] Akbari, P., Nadim, M.R., 2006, "A Review of Wave Rotor Technology and Its Applications", *Journal of Engineering for Gas Turbines and Power*, Vol. 128, pp. 717–735.
- [10] Weber, H.P., 1992, "Wave Engine Aerothermodynamic Design", *Journal of Engineering for Gas Turbines and Power*, Vol. 114, pp. 790-796.
- [11] Wilson J., 1998, "An Experimental Determination of Losses in a Three-Port Wave Rotor", *Journal of Engineering for Gas Turbine and Power*, vol.120 pp. 833-842.
- [12] Koji OKAMOTO, Toshio NAGASHIMA, and Susumu TERAMOTO, 2004, "MULTI-PASSAGE GASDYNAMIC INTERACTIONS IN WAVE ROTOR", 24TH INTERNATIONAL CONGRESS OF THE AERONAUTICAL SCIENCES
- [13] Akbari, P., Nalim, M.R., Donovan, E.S. and Snyder, P.H., 2008, "Leakage

Assessment of Pressure-Exchange Wave Rotors”, Journal of Propulsion and Power, Vol. 24, NO.4: pp. 732–740.

- [14] *Wilson, J., and Paxson, D. E., 1993, “Jet Engine Performance Enhancement Through Use of a Wave-Rotor Topping Cycle,” NASA Report, No. NASA-TM- 4486.*
- [15] *Welch, G. E., Jones, S. M., and Paxson, D. E., 1995, “Wave Rotor-Enhanced Gas Turbine Engines”, NASA Report, AIAA Paper 95-2799*
- [16] *Akbari, P., Müller, N., 2005, “Wave Rotor Research Program at Michigan State University”, 41st AIAA/ASME/SAE/ASEE Joint Propulsion Conference and Exhibit, AIAA 2005-3844*
- [17] *Shi Deng, Koji Okamoto and Susumu Teramoto, 2015, “Numerical investigation of heat transfer effects in small wave rotor”, Journal of Mechanical Science and Technology 29 (3) (2015) 939~950*
- [18] *Azoury, P. H., “An Introduction to the Dynamic Pressure Exchanger,” Proc. Inst. Mech. Eng., 180(18), Part 1, 1965-1966, pp. 451–480.*
- [19] *Kentfield, J. A. C., “The Pressure Exchanger, An Introduction Including a Review of the Work of Power Jets (R&D) Ltd.,” Proceedings ONR/NAVAIR Wave Rotor Research and Technology Workshop, Naval Postgraduate School, Monterey, CA, Report NPS-67-85-008, 1985, pp. 9–49.*
- [20] *Akbari, P., Nalim, M. R., and Müller, N., “A Review of Wave Rotor Technology and Recent Developments,” J. Engineering for Gas Turbines and Power, Vol. 128, No. 4, 2006, pp. 717-735.*
- [21] *Zauner, E., Chyou, Y. P., Walraven, F., and Althaus, R., “Gas Turbine Topping Stage Based on Energy Exchangers: Process and Performance,” ASME Paper 93-GT-58, International Gas Turbine Congress, Cincinnati, OH, 1993.*
- [22] *Paxson, D. E., Wilson, J., and Welch, G. E., “Comparison Between Simulated and*

Experimentally Measured Performance of a Four Port Wave Rotor,” NASA/TM-2007-214985, ARL-TR-4202, AIAA Paper-2007-5049, 43rd Joint Propulsion Conference, Cincinnati, OH, 2007.

[23] Welch, G. E., Paxson, D. E., Wilson, J., and Snyder, P. H., “Wave-Rotor-Enhanced Gas Turbine Engine Demonstrator,” NASA/TM-1999-209459, ARL-TR-2113, Gas Turbine Operation and Technology for Land, Sea and Air Propulsion and Power Systems Symposium, NATO, Ottawa, Canada, 1999.

[24] Weber, R., “A Pressure-Wave Machine with Integrated Constant-Volume Combustion,” Swiss Energy Research Report 1977-1997, National Foundation for Energy Research, Berne, Switzerland, Project No. 426, pp. 142-153.

[25] Akbari, P., Nalim, M. R., and Müller, N., “A Review of Wave Rotor Technology and Recent Developments,” *J. Engineering for Gas Turbines and Power*, Vol. 128, No. 4, 2006, pp. 717-735.

[26] Akbari, P., and Nalim, M. R., “Review of Recent Developments in Wave Rotor Combustion Technology,” *J. Propulsion and Power*, Vol. 25, No.4, 2009, pp. 833-844

[27] Nalim, M. R., “Assessment of Combustion Modes for Internal Combustion Wave Rotors,” *Journal of Engineering for Gas Turbines and Power*, Vol. 121, No. 2, 1999, pp. 265-271.

[28] Nalim, M. R., and Paxson, D. E., “A Numerical Investigation of Premixed Combustion in Wave Rotors,” *Journal of Engineering for Gas Turbines and Power*, Vol. 119, No. 3, 1997, pp. 668-675.

[29] Nalim, M. R., “Longitudinally Stratified Combustion in Wave Rotors,” *Journal of Propulsion and Power*, Vol. 16, No. 6, 2000, pp. 1060-1068.

[30] Snyder, P. H., Alparslan, B., and Nalim, M. R., “Wave Rotor Combustor Test Rig

Preliminary Design,” ASME Paper IMECE2004-61795, International Mechanical Engineering Congress, Anaheim, CA, 2004.

- [31] Akbari, P., Nalim, M.R., and Snyder, P.H., “Numerical Simulation and Design of a Combustion Wave Rotor for Deflagrative and Detonative Propagation,” *AIAA Paper 2006-5134, 42nd Joint Propulsion Conference, Sacramento, CA, 2006.*
- [32] Paxson, D.E., “A General Numerical Model for Wave Rotor Analysis,” *NASA TM-105740, 1992.*
- [33] Paxson, D.E., “Comparison Between Numerically Modeled and Experimentally Measured Wave-Rotor Loss Mechanisms,” *Journal of Propulsion and Power, Vol. 11, No.5, 1995.*
- [34] Paxson, D.E., “Numerical Simulation of Dynamic Wave Rotor Performance,” *Journal of Propulsion and Power, Vol.12, No.5, 1996.*
- [35] Elharis, T.M., “A Multi-step Reaction Model for Stratified-Charge Combustion in Wave Rotors,” *M.S.Thesis, Indiana University-Purdue University Indianapolis, 2011.*
- [36] Matsutomi, Y., Meyer, S., Wijeyakulasuriya, S.D., Izzy, Z., Nalim, M.R., Shimo, M., Kowalkowski, M., and Snyder, P.H., “Experimental Investigation on the Wave Rotor Constant Volume Combustor,” *AIAA 2010-7043, 46th Joint Propulsion Conference, Nashville, TN, 2010.*
- [37] Snyder, P. H., Elharis, T. M., Wijeyakulasuriya, S. D., Nalim, M. R., Matsutomi, Y., and Meyer, S., “Pressure Gain Combustor Component Viability Assessment Based on Initial Testing,” *AIAA-2011-5749, 47th Joint Propulsion Conference, San Diego, CA, July 2011.*
- [38] Snyder P. H. and Nalim, M. R., “Wave Rotor Pressure Gain Combustion Rig Performance Assessment,” *33rd JANNAF Air-Breathing Propulsion Conference,*

Joint Army Navy NASA Air Force interagency propulsion committee Paper 2746, Monterey, CA, 2012

- [39] *Wilson, J. and Paxson, D. E., 1993, "Jet Engine Performance Enhancement Through Use of a Wave-Rotor Topping Cycle," NASA TM-4486*
- [40] *Akbari, P., Müller, N., 2003, "PERFORMANCE INVESTIGATION OF SMALL GAS TURBINE ENGINES TOPPED WITH WAVE ROTORS", 39th AIAA/ASME/SAE/ASEE Joint Propulsion Conference and Exhibit, AIAA 2003-4414.*
- [41] *Iancu, F., Piechna, J., Müller, N., 2008, "Basic design scheme for wave rotors", Shock Waves (2008) 18: pp. 365–378.*
- [42] https://en.wikipedia.org/wiki/Boundary_layer#Aerodynamics
- [43] *Vittorio Verda, Adriano Sciacovelli, Romano Borchellini, 2013, "Numerical Design of Thermal Systems", ISBN 978-88-7992-387-3.*
- [44] https://en.wikipedia.org/wiki/Law_of_the_wall